# Effects of protocol and obesity on dose conversion factors in adult body CT

Xiang Li
*Carl E. Ravin Advanced Imaging Laboratories, Department of Radiology, Duke University Medical Center, Durham, North Carolina 27705*

Ehsan Samei
*Carl E. Ravin Advanced Imaging Laboratories, Department of Radiology, Medical Physics Graduate Program, Departments of Physics, Biomedical Engineering, and Electrical and Computer Engineering, Duke University Medical Center, Durham, North Carolina 27705*

Cameron H. Williams
*School of Medicine, Duke University Medical Center, Durham, North Carolina 27710*

W. Paul Segars
*Carl E. Ravin Advanced Imaging Laboratories, Department of Radiology, Medical Physics Graduate Program, Duke University Medical Center, Durham, North Carolina 27705*

Daniel J. Tward, Michael I. Miller, and J. Tilak Ratnanather
*Center for Imaging Science and Institute for Computational Medicine, The Johns Hopkins University, Baltimore, Maryland 21218*

Erik K. Paulson
*Department of Radiology, Duke University Medical Center, Durham, North Carolina 27710*

Donald P. Frush
*Department of Radiology, Medical Physics Graduate Program, Duke University Medical Center, Durham, North Carolina 27710*

(Received 2 February 2012; revised 14 August 2012; accepted for publication 4 September 2012; published 8 October 2012)

**Purpose:** In computed tomography (CT), organ dose, effective dose, and risk index can be estimated from volume-weighted CT dose index ($CTDI_{vol}$) or dose-length product (DLP) using conversion coefficients. Studies have investigated how these coefficients vary across scanner models, scan parameters, and patient size. However, their variability across CT protocols has not been systematically studied. Furthermore, earlier studies of the effect of patient size have not included obese individuals, which currently represent more than one-third of U.S. adults. The purpose of this study was to assess the effects of protocol and obesity on dose and risk conversion coefficients in adult body CT.

**Methods:** Whole-body computational phantoms were created from clinical CT images of six adult patients (three males, three females), representing normal-weight patients and patients of three obesity classes. Body CT protocols at our institution were selected and categorized into ten examination categories based on anatomical region examined. A validated Monte Carlo program was used to estimate organ dose. Organ dose estimates were normalized by $CTDI_{vol}$ and size-specific dose estimate (SSDE) to obtain organ dose conversion coefficients (denoted as $h$ and $h_{ss}$ factors, respectively). Assuming each phantom to be 20, 40, and 60 years old, effective dose and risk index were calculated and normalized by DLP to obtain effective dose and risk index conversion coefficients (denoted as $k$ and $q$ factors, respectively). Coefficient of variation was used to quantify the variability of each conversion coefficient across examination categories. The effect of obesity was assessed by comparing each obese phantom with the normal-weight phantom of the same gender.

**Results:** For a given organ, the variability of $h$ factor across examination categories that encompassed the entire organ volume was generally within 15%. However, $k$ factor varied more across examination categories (15%–27%). For all three ages, the variability of $q$ factor was small for male (<10%), but large for female phantoms (21%–43%). Relative to the normal-weight phantoms, the reduction in $h$ factor (an average across fully encompassed organs) was 17%–42%, 17%–40%, and 51%–63% for obese-class-I, obese-class-II, and obese-class-III phantoms, respectively. $h_{ss}$ factor was not independent of patient diameter and generally decreased with increasing obesity. Relative to the normal-weight phantoms, the reduction in $k$ factor was 12%–40%, 14%–46%, and 44%–59% for obese-class-I, obese-class-II, and obese-class-III phantoms, respectively. The respective reduction in $q$ factor was 11%–36%, 17%–42%, and 48%–59% at 20 years of age and similar at other ages.

**Conclusions:** In adult body CT, dose to an organ fully encompassed by the primary radiation beam can be estimated from $CTDI_{vol}$ using a protocol-independent conversion coefficient. However, fully encompassed organs only account for 50% ± 19% of $k$ factor and 46% ± 24% of $q$ factor. Dose

received by partially encompassed organs is also substantial. To estimate effective dose and risk index from DLP, it is necessary to use conversion coefficients specific to the anatomical region examined. Obesity has a significant effect on dose and risk conversion coefficients, which cannot be predicted using body diameter alone. SSDE-normalized organ dose is not independent of diameter. SSDE itself generally overestimates organ dose for obese patients. © *2012 American Association of Physicists in Medicine*. [http://dx.doi.org/10.1118/1.4754584]

Key words: CT, radiation, dose, organ dose, effective dose, risk index, size-specific dose estimate, protocol, obesity, Monte Carlo, computational phantom, XCAT

## I. INTRODUCTION

Radiation protection is an important issue in computed tomography (CT).[1–3] Due to the large number of CT examinations performed every year and the relatively high radiation exposure associated with each examination, CT currently accounts for half of the medical radiation exposure to the U.S. population.[4] The importance of radiation protection in CT necessitates accurate dose assessment for this imaging modality.[5] Accurate estimation of dose is needed to monitor the appropriate use of CT radiation, to establish diagnostic reference levels, and to optimize CT protocols.

Currently two types of dose quantities are used in CT: quality assurance dose quantities (e.g., CT dose index and dose-length product) and patient dose quantities (e.g., organ dose, effective dose, and risk index[6,7]). Quality assurance dose quantities, typically, volume-weighted CT dose index ($CTDI_{vol}$) and dose-length product (DLP), are displayed on the CT scanner console prior to a patient's CT scan and can be saved in a dose report after the scan is completed. Efforts are underway to include these quality assurance dose quantities in digital imaging and communications in medicine (DICOM) structured reporting. To allow patient dose quantities to be conveniently estimated from quality assurance dose quantities, conversion coefficients have been developed.[7–11] The conversion coefficient from DLP to effective dose is commonly referred to as the "*k* factor."[11,12] In our earlier work,[7] we promoted the use of risk index as a valuable metric and denoted the conversion coefficient from DLP to risk index as the "*q* factor." Here, we denote the conversion coefficient from $CTDI_{vol}$ to organ dose as the "*h* factor" (a glossary of symbols used in the paper is given in Table I). The "*h* factor" is equivalent to the quantity $nD_{P,S,O}$ used in the work of Turner *et al.*[10]

TABLE I. Glossary of symbols.

| Symbol | Definition |
|---|---|
| $h$ | Conversion coefficient from $CTDI_{vol}$ to organ dose |
| $\langle h \rangle_{inside}$ | Average of $h$ across organs fully inside the scan coverage[a] |
| $h_{ss}$ | Conversion coefficient from SSDE to organ dose |
| $\langle h_{ss} \rangle_{inside}$ | Average of $h_{ss}$ across organs fully inside the scan coverage[a] |
| $k$ | Conversion coefficient from DLP to effective dose |
| $q$ | Conversion coefficient from DLP to risk index |

[a]Also referred to as organs fully encompassed by the primary radiation beam.

Earlier studies indicated that *k* factors are generally independent of scanner models (up to 64 rows of detectors or approximately 40 mm beam collimation).[8,9] Such is also the case for *h* factors provided that the organs are fully encompassed by the primary radiation beam.[13] Our recent study in pediatric chest CT[7] also showed that *k* factor, *q* factor, and the *h* factor for a fully encompassed organ vary little (<10%) across several scan parameters including collimation, pitch, and tube potential. Furthermore, recent studies in chest and abdominal CT have suggested that *h*, *k*, and *q* factors may be expressed in terms of patient size, age, and gender using simple analytical equations.[7,10] Having these desirable properties, the dose and risk conversion coefficients provide a practical method for obtaining more individualized dose and risk estimates for CT patients.

However, the available *h*, *k*, and *q* factors are limited to a small number of CT protocols that cover an entire region of the body (e.g., head, neck, chest, and abdomen or abdomen/pelvis). While such examinations are the most frequently used, with the increasing speed of multidetector array CT systems, multiphase CT protocols that cover only a single organ or a subregion of the body have also become routine. Examples are multiphase liver and renal protocols. At present, dose and risk conversion coefficients are largely unavailable for such examinations. It is unclear, for instance, whether the *k* factor developed for an abdominal CT examination can effectively substitute those for the examinations of the kidneys or the adrenal glands. Given the large number of CT protocols in use clinically, especially for adult patients, it is necessary to know if and how much *h, k,* and *q* factors vary across CT protocols and whether protocol-independent conversion coefficients are feasible.

Recently, AAPM Task Group 204 proposed a new dose quantity for body CT, size-specific dose estimate (SSDE), defined as $CTDI_{vol}$ multiplied by a patient size-specific adjustment factor.[14] By taking patient size into account, SSDE is a significant step beyond the conventional $CTDI_{vol}$ and has utility in CT dose monitoring and protocol optimization. By definition, SSDE approximates the average dose across the field of view (cross section) of a phantom representing the size of the patient, resulting from a helical scan or a series of axial scans. As such, SSDE is potentially a good estimator of dose to organs fully inside the scan coverage. Furthermore, because SSDE takes patient size into account, the conversion coefficients from SSDE to organ dose are potentially independent of patient size. However, these desirable properties of SSDE have not been tested for a variety of body protocols. Furthermore, given that more than one-third of U.S. adults (35.7%)

are obese individuals,[15] it is necessary to test whether these desirable properties of SSDE also apply to obese patients.

In this study, we focused on adult body CT examinations (i.e., non-neurological, noncardiac, nonmusculoskeletal examination). Our goals were (1) to extend the $h$, $k$, and $q$ factors to a wide range of body CT protocols by using realistic computational phantoms and Monte Carlo dose simulations, (2) to examine the variability of these conversion coefficients across protocols, and (3) to assess the effect of obesity on these conversion coefficients.

## II. MATERIALS AND METHODS

### II.A. Patients and computational phantoms

The study population consisted of six adult patients (mean age, 46 years; age range, 31–58 years; mean weight, 86 kg; weight range, 66–117 kg; mean height, 173 cm; height range, 156–180 cm), three males (66–117 kg) and three females (68–105 kg). They were retrospectively selected from our clinical database of patients who underwent a complete chest-abdomen-pelvis CT examination. The criteria for selection were that the examinations were normal or contained findings that would not affect organ size, position, and morphology, as verified by a radiologist (20 years of experience in adult body imaging).

The clinical CT images of each patient were used as the basis to create a whole-body computational phantom. The initial anatomy was defined by segmenting the patient's CT data using a graphical software application developed in our laboratory. Body surface, skeleton, and lungs were semi-automatically segmented based on CT number thresholding. The heart, kidneys, liver, stomach, gallbladder, and spleen were manually contoured in each CT slice. From the segmented masks, three-dimensional triangulated polygon models were created by applying the marching cubes algorithm.[16] Three-dimensional nonuniform rational B-spline (NURBS) surfaces were then fit to the polygon models using NURBS modeling software (Rhinoceros, McNeel North America, Seattle, WA) to create the initial patient-specific phantom.

This initial phantom covered only the regions over which the CT data were acquired, namely the chest, abdomen, and pelvis. To complete the initial phantom, the head, arms, and legs were created by transforming the corresponding structures in an existing extended cardiac-torso (XCAT) model,[17] which represented a 50th percentile reference adult. Specifically, the head, arms, and legs of the reference model were scaled so as to match specific body dimensions (head circumference, arm and leg thicknesses) determined for the particular patient based on the patient's characteristics. The desired body dimensions were obtained using the PeopleSize program (Open Ergonomics Ltd.). After scaling the head, arms, and legs to match the body type of the patient, they were placed manually onto the rest of the anatomy using the segmented skeleton as a guide.

Following the addition of head, arms, and legs, the large deformation diffeomorphic metric mapping (LDDMM) framework[18] was used to fill in the rest of the anatomy by nonrigidly transforming the reference phantom to match the limited framework defined by the initial patient-specific phantom.[19–21] Using this method, a patient-specific XCAT

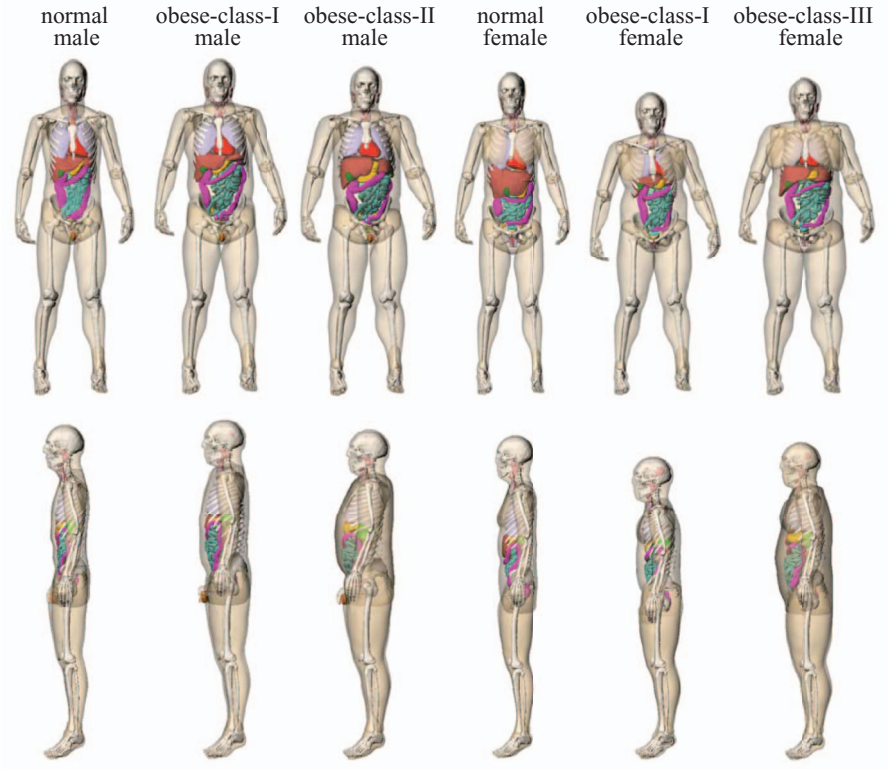


FIG. 1. Surface-rendered views of the computational phantoms of the six patients in this study.

TABLE II. Characteristics of the voxelized phantoms of the six patients in this study.

| Phantom | Gender | Height (cm) | Weight (kg) | BMI[a] | BMI classification[a] |
|---|---|---|---|---|---|
| 1 | Male | 182.5 | 74.6 | 22.4 | Normal |
| 2 | Male | 184.6 | 107.3 | 31.5 | Obese class I |
| 3 | Male | 181.8 | 124.4 | 37.6 | Obese class II |
| 4 | Female | 176.6 | 76.4 | 24.5 | Normal |
| 5 | Female | 166.3 | 90.7 | 32.8 | Obese class I |
| 6 | Female | 174.9 | 128.5 | 42.0 | Obese class III |

[a]BMI (body mass index) = weight (kg)/height$^2$ (m). BMI classification is based on that used by the World Health Organization: normal if BMI = 18.50–24.99, overweight if BMI = 25–29.99, obese class I if BMI = 30.00–34.99, obese class II if BMI = 35.00–39.99, and obese class III if BMI ≥ 40.00 (Ref. 47).

phantom was created that contained thousands of structures. The volumes of the transformed organs (i.e., organs that were not patient-specific) were checked against age-interpolated values from ICRP Publication 89.[22] Figure 1 illustrates the phantoms created using the process described above.

For input into Monte Carlo simulations, the NURBS-based phantoms were each "positioned" on a model of the CT table in a supine position with arms elevated above the head to mimic the usual patient posture during body CT examinations. They were voxelized at 3.45-mm isotropic resolution with 43 (male) or 44 (female) organs labeled by unique integer identification numbers. A list of these organs has been reported in our earlier publication.[6] They included most of the radiosensitive organs defined by ICRP Publication 103.[23] Table II summarizes the body measurements and body mass index (BMI) classification of the voxelized phantoms.

### II.B. Body CT protocols and examination categories

Currently at our institution, routine adult (>18 years) body CT consists of 46 protocols, including both single-phase and multiple-phase protocols. Despite the large number, many protocols examine similar anatomical regions and share the same scan parameters (differing in terms of breathing instruction, the use of oral or intravenous iodinated contrast, and reconstruction and reformation parameters).

We grouped these protocols into examination categories based on the anatomical regions examined and selected ten examination categories, corresponding to the majority of the body protocols (Table III). At our institution, these protocols share a common set of scan parameters on a 64-slice CT system (LightSpeed VCT scanner, GE Healthcare, Waukesha, WI): tube voltage of 120 kVp, pitch of 1.375, beam collimation of 40 mm, and large body scan field-of-view.

### II.C. Radiation dose and cancer risk index estimation

For each phantom and examination category, organ dose was simulated for the above scan parameters using a validated Monte Carlo program. The Monte Carlo program was previously developed for dose simulation on a 64-slice CT system (LightSpeed VCT, GE Healthcare, Waukesha, WI).[24] The program explicitly modeled the geometry of the CT system, the three-dimensional geometry of the bowtie filters, and the trajectories of x-ray tube motion during axial and helical scans. The accuracy of the simulated dose was previously validated in a cylindrical phantom and in two anthropomorphic phantoms for both axial and helical scanning modes. Simulations were found to agree with measurements within 1%–11% on average and 5%–17% maximum.[24]

For each simulation, the total scan length included the image coverage (2nd column of Table III) plus the over-ranging distance (additional scan length necessary for data interpolation in helical reconstruction).[25] For the set of scan parameters and scanner model investigated in this study (Sec. II.B), the over-ranging distance was 6.40 cm.[7]

For most organs and tissues, energy deposition was tallied and used to calculate dose. Eighty million ($8 \times 10^7$) photon histories were used to simulate each examination of each phantom, resulting in relative dose errors of less than 1% for all organs in the scan coverage and less than 4% for other organs. To assess dose to the red bone marrow, volume-averaged photon fluence spectrum was tallied individually at each skeletal site and used to calculated dose to the red bone marrow using fluence-to-dose conversion coefficients.[26] A single red marrow dose was then calculated as its skeletal average using the age-dependent fractional distribution of active marrow tabulated in ICRP Publication 89.[22] Dose to the bone surface was approximated by the mass-weighted average of dose to the homogenous bones.[27]

The estimated organ dose values were used to calculate effective dose as

$$E = \sum_T w_T H_T, \tag{1}$$

where $H_T$ is the equivalent dose for organ/tissue $T$ and $w_T$ is the tissue weighting factor defined by ICRP Publication 103.[23] All radiosensitive organs defined by the ICRP publication regardless of their locations relative to the primary radiation beam were included in Eq. (1). Dose to radiosensitive organs that were not explicitly modeled was approximated by dose to neighboring organs.[6] In principle, effective dose calculation should employ gender-averaged organ dose values.[23] As the computational phantom of each patient only had the reproductive organs (testes, prostate, ovaries, and uterus/cervix) of one gender, dose to the testes or the ovaries was used to approximate gender-averaged dose to the gonads, and dose to the "reminder tissues" of one gender was used to approximate gender-averaged dose to the "reminder tissues." The effective dose value calculated in this way represented the effective dose to a patient population (including both genders) that has similar anatomy and body habitus as the patient whose organ dose values were used in the effective dose calculation. This approach most reasonably implemented the ICRP definition of effective dose.

The estimated organ dose values were also used to calculate risk index,[6,7,28] defined as

$$\text{Risk index} = \sum_T r_T(\text{gender}, \text{age}) H_T, \tag{2}$$

TABLE III. Body CT protocols investigated in this study. The protocols were grouped into examination categories based on anatomical regions examined.

| Examination category | Image coverage | Clinical protocols |
|---|---|---|
| Chest-abdomen-pelvis | Start: 1 cm above lung apex<br>End: 1 cm below inferior ischium | Chest abdomen pelvis—trauma |
| Chest | Start: 1 cm above lung apex<br>End: 1 cm below lung base | Standard chest<br>Standard chest with contrast<br>Pulmonary embolism<br>Chest trauma<br>Low-dose chest<br>Airway<br>Bronchiolitis obliterans<br>Bronchiectasis—inspiration<br>Bronchiectasis—expiration<br>Interstitial lung disease—inspiration (supine)<br>Interstitial lung disease—expiration (supine)<br>Follow up interstitial lung disease |
| Abdomen-pelvis | Start: 1 cm above superior liver<br>End: 1 cm below inferior ischium | Abdomen pelvis<br>Abdomen pelvis—acute<br>Abdomen pelvis—trauma<br>Chest abdomen pelvis—abdomen-pelvis part<br>Colonography—supine scan<br>Small bowel<br>Valsalva abdomen pelvis |
| Abdomen | Start: 1 cm above superior liver<br>End: 1 cm below superior iliac crest | Cholangiocarcinoma—contrast enhanced phase<br>Hepatic resection—venous phase<br>Pancreas—venous phase |
| Pelvis | Start: 1 cm above superior iliac crest<br>End: 1 cm below inferior ischium | Cystogram |
| Adrenal | Start: 1 cm above superior adrenals<br>End: 1 cm below inferior adrenals | Adrenal—precontrast phase<br>Adrenal—post-contrast phase<br>Adrenal—delayed phase |
| Liver | Start: 1 cm above superior liver<br>End: 1 cm below inferior liver | Cholangiography<br>Cirrhosis—arterial phase<br>Cirrhosis—venous phase<br>Cirrhosis—delayed phase<br>Dual liver—arterial phase<br>Dual liver—venous phase |
| Kidney | Start: 1 cm above superior kidney<br>End: 1 cm below inferior kidney | Renal cell cancer—precontrast phase<br>Renal CT angiography—noncontrast phase<br>Renal CT angiography—arterial phase<br>Renal donor—noncontrast phase<br>Renal donor—arterial phase |
| Liver-to-kidney | Start: 1 cm above superior liver<br>End: 1 cm below inferior kidney | Dual renal—nephrographic phase<br>Renal cell cancer—arterial phase<br>Renal cell cancer—venous phase |
| Kidney-to-bladder | Start: 1 cm above superior kidney<br>End: 1 cm below inferior bladder | Dual renal—precontrast phase<br>Dual renal—excretory phase<br>Renal stone |

where $r_T$ is the gender-specific, age-specific, and tissue-specific risk coefficient (cases/100 000 exposed to 0.1 Gy) for lifetime attributable risk of cancer incidence tabulated in the BEIR VII report.[29] All radiosensitive organs regardless of their locations relative to the primary radiation beam were included the calculation. More details about risk index calculation have been reported in an earlier publication.[6]

To assess the effect of obesity independent of age, each computational phantom was assumed to represent individuals at three ages: 20, 40, and 60 years of age. In ICRP Publication 89,[22] age-dependent fractional distribution of red marrow is only available up to 40 years of age, we assumed the distribution to stay unchanged from 40 to 60 years of age.

### II.D. Calculation of *h*, *k*, and *q* factors

The organ dose estimates obtained for each phantom and each examination category were normalized by the

corresponding $CTDI_{vol}$ to calculate the $h$ factors. The effective dose and risk index were normalized by the corresponding DLP to obtain the $k$ and $q$ factors, respectively. The $CTDI_{vol}$ was calculated from the technical reference manual of the CT scanner model in this study using the tables of $CTDI_{100}$ and technique adjustment factors. DLP was calculated as the product of $CTDI_{vol}$ and total scan length (image coverage plus overranging distance). The $CTDI_{vol}$ and DLP calculated in this way agreed with those from patients' dosimetry reports to within about 5%. For the set of scan parameters and scanner model investigated in this study (Sec. II.B), the $CTDI_{vol}$ was 6.01 mGy/100 mAs.

To test whether SSDE is a close approximation to organ dose and whether the conversion coefficients from SSDE to organ dose (denoted as $h_{ss}$ factor) are independent of patient size, the organ dose estimates for each phantom were also normalized by SSDE. SSDE was determined as

$$\mathrm{SSDE(mGy/100\,mAs)} = \frac{\mathrm{SSDE}}{\mathrm{CTDI_{vol}}}(d) \times \mathrm{CTDI_{vol}(mGy/100\,mAs)}. \quad (3)$$

In Eq. (3), $d$ is the average diameter of a body region (trunk, chest, abdomen-pelvis, abdomen, or pelvis) calculated for each phantom as

$$d = 2\sqrt{\frac{\langle A\rangle_{\mathrm{region}}}{\pi}}, \quad (4)$$

where $\langle A\rangle_{\mathrm{region}}$ is the average cross-sectional area of the body region, and $\frac{\mathrm{SSDE}}{\mathrm{CTDI_{vol}}}(d)$ is the functional dependence of the ratio SSDE/$CTDI_{vol}$ on effective diameter, i.e., the exponential equation in Fig. 4 of AAPM Report No. 204.[14] To calculate SSDE for the chest-abdomen-pelvis, chest, abdomen-pelvis, abdomen, and pelvis examinations, the average diameters of the respective regions were used. To calculate SSDE for the adrenal, liver, kidney, and liver-to-kidney examinations, average diameter of the abdomen region was used. Lastly, for the kidney-to-bladder examination, average diameter of the abdomen-pelvis region was used.

### II.E. Effects of protocol and obesity

For each organ, we calculated the variability of $h$ factor across categories of examinations that encompassed the entire organ volume inside the primary radiation beam. For example, the variability of $h$ factor was assessed for the lungs across two examination categories: chest and chest-abdomen-pelvis examination categories. In these two categories, the entire lung volume was inside the scan coverage. Another example is the small intestine, for which the variability of $h$ factor was assessed across three examination categories: chest-abdomen-pelvis, abdomen-pelvis, and kidney-to-bladder examinations. The variability of $k$ and $q$ factors was assessed for each phantom across all ten examination categories. The coefficient of variation (standard deviation $\times$ 100%/mean)[30] was used to quantify the variability.

We considered protocol-independent conversion coefficients to be feasible if the variability across protocols was smaller than the variability across scanner models, scan parameters, and patients within the same cohort (defined as patients having body diameters within 1 cm of one another). Earlier studies showed that $k$ factors and the $h$ factors for fully encompassed organs vary less than 10% across scanner models and scan parameters.[7–9,13] To quantify within-cohort variability, the data published by Li *et al.* for 30 pediatric chest CT patients[7] were examined. Specifically, multiple patient cohorts were identified from the 30 patients, each of which consisted of 4–9 patients having chest diameters ranged within 1 cm of one another. Among fully encompassed organs, thyroid and breasts had the largest within-cohort variability in $h$ factor of 7%–15% and 19%–24%, respectively. The within-cohort variability in $k$ factor ranged between 3%–12%. Based on this analysis, we set a variability threshold of 20% for $h$ and $k$ factors, below which protocol-independent conversion coefficients were deemed acceptable. Within-cohort variability in $q$ factor could not be reliably assessed because the numbers of patients within each cohort (same gender, similar diameter, and age) were too small. The same threshold of 20% was also applied to $q$ factor.

To assess the effect of obesity, each obese phantom was compared with the normal-weight phantom in the same gender category.

## III. RESULTS

Because dose to the red marrow was calculated as its skeletal average using the age-dependent fractional distribution of red marrow, there existed small differences in $k$ factors (<0.7%) and $h$ factors for red marrow (<11%) between 20 and 40 years of age. There was no difference between 40 and 60 years of age because these two ages were assumed to have identical red marrow distribution. The $k$ factors and $h$ factors for red marrow reported thereafter refer to values obtained at 20 years of age.

### III.A. Effect of protocol

For each phantom and examination category, the $h$ factors obtained for all the organs, including those that are not totally encompassed by the primary beam, are given in Tables XII–XVII of the Appendix. For each organ, the variability of $h$ factor across examination categories that cover the entire organ volume (i.e., variability along the row direction in Tables XII–XVII) is summarized in Table IV. The variability was generally less than 15%. The exceptions were the testes in the obese-class-II male phantom (variability = 18%) and the gall bladder in the obese-class-III female phantom (variability = 16%). In contrast to the variability across examination categories, within a given examination category, the variability of $h$ factor across fully encompassed organs was higher (Table V). The highest variability (47%) was found for the pelvic examination of the obese-class-II male phantom, where the $h$ factor for the testes was more than double that for the prostate. With this exception, the variability of $h$ factor across fully encompassed organs was less than 28%. For a given phantom, $h_{ss}$ differed from $h$ only by a scaling

TABLE IV. For given phantom and organ, variability of $CTDI_{vol}$-to-organ dose conversion coefficients ($h$ factors, unitless) across examination categories that covered the entire organ volume[a].

| | Male | | | Female | | |
|---|---|---|---|---|---|---|
| | Normal (%) | Obese class I (%) | Obese class II (%) | Normal (%) | Obese class I (%) | Obese class III (%) |
| Thyroid | – | – | – | – | 0.4 | – |
| Trachea-bronchi | 1 | 1 | 1 | 1 | 1 | – |
| Breasts | 0.3 | 0.6 | 0.7 | 0.5 | 1.6 | 1.0 |
| Thymus | 0.7 | 0.4 | 0.8 | 0.5 | 0.5 | 0.7 |
| Esophagus | 2 | 3 | 3 | 1 | 2 | 2 |
| Lungs | 2 | 2 | 2 | 2 | 2 | 2 |
| Heart | 2 | 3 | 2 | 2 | 3 | 2 |
| Liver | 5 | 4 | 5 | 3 | 5 | 6 |
| Gall bladder | 8 | 9 | 11 | 4 | 9 | 16 |
| Spleen | 7 | 5 | 8 | 7 | 6 | 9 |
| Stomach | 8 | 11 | 11 | 5 | 3 | 11 |
| Pancreas | 8 | 9 | 11 | 5 | 9 | 12 |
| Adrenal glands | 9 | 11 | 10 | 9 | 9 | 12 |
| Kidneys | 6 | 5 | 6 | 4 | 4 | 7 |
| Large intestine | 2 | 1 | 2 | 2 | 3 | 4 |
| Small intestine | 2 | 2 | 1 | 1 | 2 | 2 |
| Prostate | 7 | 9 | 6 | – | – | – |
| Bladder | 8 | 7 | 2 | 4 | 6 | 4 |
| Testes | 11 | 6 | 18 | – | – | – |
| Ovaries | – | – | – | 4 | 3 | 3 |
| Uterus | – | – | – | 3 | 2 | 3 |
| Vagina | – | – | – | 1 | 9 | 1 |

[a]Variability is quantified by the coefficient of variation (standard deviation × 100%/mean).

TABLE V. For given phantom and examination category, variability of $CTDI_{vol}$-to-organ dose conversion coefficients ($h$ factors, unitless) across fully encompassed organs (i.e., organs completely inside the scan coverage)[a].

| | Male | | | Female | | |
|---|---|---|---|---|---|---|
| | Normal (%) | Obese class I (%) | Obese class II (%) | Normal (%) | Obese class I (%) | Obese class III (%) |
| Chest-abdomen-pelvis | 12 | 16 | 18 | 16 | 18 | 23 |
| Chest | 8 | 15 | 16 | 12 | 20 | 21 |
| Abdomen-pelvis | 16 | 16 | 26 | 14 | 9 | 17 |
| Abdomen | 11 | 13 | 20 | 10 | 10 | 19 |
| Pelvis | 26 | 28 | 47 | 4 | 5 | 5 |
| Adrenal | 16 | 18 | 22 | 19 | 18 | 15 |
| Liver | 12 | 13 | 21 | 10 | 11 | 19 |
| Kidney | 12 | 15 | 23 | 13 | 13 | 17 |
| Liver-to-kidney | 12 | 13 | 20 | 10 | 10 | 20 |
| Kidney-to-bladder | 18 | 22 | 27 | 16 | 12 | 17 |

[a]Variability is quantified by the coefficient of variation (standard deviation × 100%/mean).

factor (the ratio between $CTDI_{vol}$ and SSDE). As such, $h_{ss}$ and $h$ have the same variability across examination categories that encompassed the entire organ volume. For a given examination category, they also have the same variability across fully encompassed organs.

For a given phantom, $k$ factor varied considerably across different examination categories (Table VI). The coefficient of variation ranged between 15% and 27% for the six phantoms. Among the ten examination categories, pelvic examination had the lowest $k$ factor for all the phantoms, whereas examinations of the chest or the adrenal glands had the highest $k$ factor for all but the obese-class-II male phantom, for which the liver examination was associated with the highest $k$ factor. If the $k$ factor for the abdomen-pelvis examination is used to estimate the effective dose associated with an examination of the adrenal glands, the error introduced ranges from −10% for the obese-class-II male phantom to −39% for the normal-weight male phantom.

For a given male phantom, $q$ factor varied slightly across different examination categories (Table VII). The coefficient of variation ranged between 6% and 9% for the three male phantoms. In contrast, for a given female phantom, $q$ factor varied considerably across different examination categories. At 20 years of age, the coefficient of variation ranged between 36% and 43% for the three female phantoms. The

TABLE VI. DLP-to-effective dose conversion coefficients ($k$ factors, unit: mSv/mGy-cm).

| | Scan length (cm) | Male | | | Female | | |
|---|---|---|---|---|---|---|---|
| | | Normal | Obese class I | Obese class II | Normal | Obese class I | Obese class III |
| Chest-abdomen-pelvis | 71 ± 3 | 0.017 | 0.015 (−17%)[a] | 0.012 (−33%)[a] | 0.017 | 0.013 (−28%)[a] | 0.009 (−51%)[a] |
| Chest | 33 ± 3 | 0.024 | 0.020 (−17%) | 0.014 (−39%) | 0.022 | 0.019 (−12%) | 0.012 (−44%) |
| Abdomen-pelvis | 53 ± 2 | 0.016 | 0.013 (−19%) | 0.013 (−21%) | 0.016 | 0.011 (−30%) | 0.008 (−53%) |
| Abdomen | 31 ± 1 | 0.019 | 0.016 (−15%) | 0.015 (−22%) | 0.020 | 0.014 (−28%) | 0.009 (−52%) |
| Pelvis | 31 ± 1 | 0.011 | 0.009 (−19%) | 0.010 (−14%) | 0.011 | 0.007 (−40%) | 0.005 (−58%) |
| Adrenal | 15 ± 1 | 0.026 | 0.018 (−30%) | 0.014 (−46%) | 0.022 | 0.018 (−19%) | 0.011 (−51%) |
| Liver | 26 ± 2 | 0.021 | 0.018 (−18%) | 0.016 (−27%) | 0.021 | 0.017 (−21%) | 0.010 (−52%) |
| Kidney | 19 ± 1 | 0.022 | 0.016 (−28%) | 0.013 (−43%) | 0.021 | 0.014 (−34%) | 0.009 (−59%) |
| Liver-to-kidney | 27 ± 2 | 0.022 | 0.017 (−21%) | 0.015 (−31%) | 0.021 | 0.015 (−29%) | 0.010 (−53%) |
| Kidney-to-bladder | 41 ± 1 | 0.015 | 0.011 (−24%) | 0.011 (−24%) | 0.017 | 0.011 (−34%) | 0.007 (−59%) |
| Coefficient of variation | | 24% | 22% | 15% | 18% | 27% | 24% |

[a]Values in parenthesis are percent differences relative to the normal-weight phantom in the same gender category.

TABLE VII. DLP-to-risk index conversion coefficients ($q$ factors, unit: cancer incidences/million exposed/mGy-cm).

| | | Male (20-year-old) | | | Female (20-year-old) | | |
|---|---|---|---|---|---|---|---|
| | Scan length (cm) | Normal | Obese class I | Obese class II | Normal | Obese class I | Obese class III |
| Chest-abdomen-pelvis | 71 ± 3 | 1.6 | 1.3 (−18%) | 1.1 (−30%) | 3.0 | 2.2 (−28%) | 1.5 (−51%) |
| Chest | 33 ± 3 | 1.6 | 1.4 (−17%) | 1.1 (−35%) | 4.7 | 3.9 (−18%) | 2.5 (−48%) |
| Abdomen-pelvis | 53 ± 2 | 1.8 | 1.4 (−21%) | 1.3 (−27%) | 2.1 | 1.6 (−24%) | 1.0 (−52%) |
| Abdomen | 31 ± 1 | 1.7 | 1.4 (−18%) | 1.1 (−32%) | 2.6 | 2.1 (−20%) | 1.3 (−51%) |
| Pelvis | 31 ± 1 | 1.6 | 1.3 (−20%) | 1.3 (−17%) | 1.3 | 0.8 (−36%) | 0.6 (−55%) |
| Adrenals | 15 ± 1 | 2.1 | 1.5 (−28%) | 1.2 (−42%) | 2.6 | 2.2 (−16%) | 1.1 (−56%) |
| Liver | 26 ± 2 | 1.9 | 1.5 (−20%) | 1.2 (−37%) | 2.8 | 2.5 (−11%) | 1.4 (−51%) |
| Kidneys | 19 ± 1 | 1.9 | 1.4 (−26%) | 1.2 (−39%) | 2.1 | 1.6 (−23%) | 0.9 (−59%) |
| Liver-to-kidney | 27 ± 2 | 1.9 | 1.5 (−23%) | 1.2 (−38%) | 2.9 | 2.3 (−22%) | 1.4 (−53%) |
| Kidney-to-bladder | 41 ± 1 | 1.7 | 1.3 (−25%) | 1.3 (−21%) | 1.8 | 1.3 (−26%) | 0.8 (−57%) |
| Coefficient of variation | | 9% | 6% | 7% | 36% | 40% | 43% |
| | | Male (40-year-old) | | | Female (40-year-old) | | |
| | Scan length (cm) | Normal | Obese class I | Obese class II | Normal | Obese class I | Obese class III |
| Chest-abdomen-pelvis | 71 ± 3 | 1.1 | 0.9 (−18%) | 0.8 (−30%) | 1.6 | 1.2 (−28%) | 0.8 (−51%) |
| Chest | 33 ± 3 | 1.1 | 0.9 (−17%) | 0.7 (−35%) | 2.3 | 1.9 (−18%) | 1.2 (−47%) |
| Abdomen-pelvis | 53 ± 2 | 1.2 | 0.9 (−21%) | 0.9 (−27%) | 1.3 | 0.9 (−27%) | 0.6 (−52%) |
| Abdomen | 31 ± 1 | 1.2 | 0.9 (−19%) | 0.8 (−33%) | 1.6 | 1.2 (−24%) | 0.8 (−51%) |
| Pelvis | 31 ± 1 | 1.1 | 0.9 (−21%) | 0.9 (−18%) | 0.9 | 0.5 (−36%) | 0.4 (−55%) |
| Adrenals | 15 ± 1 | 1.4 | 1.0 (−27%) | 0.8 (−42%) | 1.6 | 1.2 (−21%) | 0.7 (−55%) |
| Liver | 26 ± 2 | 1.2 | 1.0 (−20%) | 0.8 (−37%) | 1.7 | 1.4 (−16%) | 0.8 (−51%) |
| Kidneys | 19 ± 1 | 1.3 | 0.9 (−25%) | 0.8 (−38%) | 1.3 | 1.0 (−28%) | 0.6 (−59%) |
| Liver-to-kidney | 27 ± 2 | 1.3 | 1.0 (−22%) | 0.8 (−38%) | 1.7 | 1.3 (−26%) | 0.8 (−52%) |
| Kidney-to-bladder | 41 ± 1 | 1.1 | 0.9 (−25%) | 0.9 (−23%) | 1.2 | 0.8 (−30%) | 0.5 (−57%) |
| Coefficient of variation | | 9% | 6% | 8% | 26% | 32% | 33% |
| | | Male (60-year-old) | | | Female (60-year-old) | | |
| | Scan length (cm) | Normal | Obese class I | Obese class II | Normal | Obese class I | Obese class III |
| Chest-abdomen-pelvis | 71 ± 3 | 0.8 | 0.7 (−19%) | 0.6 (−31%) | 1.1 | 0.8 (−27%) | 0.5 (−50%) |
| Chest | 33 ± 3 | 0.8 | 0.7 (−17%) | 0.5 (−35%) | 1.5 | 1.2 (−17%) | 0.8 (−46%) |
| Abdomen-pelvis | 53 ± 2 | 0.9 | 0.7 (−20%) | 0.6 (−28%) | 0.9 | 0.6 (−29%) | 0.4 (−52%) |
| Abdomen | 31 ± 1 | 0.9 | 0.7 (−19%) | 0.6 (−33%) | 1.1 | 0.8 (−27%) | 0.5 (−51%) |
| Pelvis | 31 ± 1 | 0.8 | 0.6 (−21%) | 0.7 (−20%) | 0.6 | 0.4 (−37%) | 0.3 (−55%) |
| Adrenals | 15 ± 1 | 1.0 | 0.7 (−27%) | 0.6 (−41%) | 1.1 | 0.8 (−25%) | 0.5 (−54%) |
| Liver | 26 ± 2 | 0.9 | 0.7 (−20%) | 0.6 (−37%) | 1.2 | 0.9 (−20%) | 0.6 (−51%) |
| Kidneys | 19 ± 1 | 0.9 | 0.7 (−25%) | 0.6 (−38%) | 1.0 | 0.7 (−32%) | 0.4 (−59%) |
| Liver-to-kidney | 27 ± 2 | 1.0 | 0.7 (−22%) | 0.6 (−38%) | 1.2 | 0.8 (−28%) | 0.6 (−52%) |
| Kidney-to-bladder | 41 ± 1 | 0.9 | 0.7 (−25%) | 0.7 (−25%) | 0.8 | 0.6 (−32%) | 0.4 (−57%) |
| Coefficient of variation | | 8% | 5% | 7% | 21% | 29% | 28% |

Note: Values in parenthesis are percent differences relative to the normal-weight phantom in the same gender category.

variability decreased slightly with increasing age, but was still above 20% at 60 years of age. Among the ten examination categories, pelvic examination had the lowest $q$ factor for all the female phantoms, whereas chest examination had the highest $q$ factor.

### III.B. Effect of obesity

To assess the effect of obesity, for given phantom and examination category, the $h$ factors for fully encompassed organs were averaged ($\langle h \rangle_{\text{inside}}$). Values of $\langle h \rangle_{\text{inside}}$ are given in Table VIII. Relative to the normal-weight male phantom, $\langle h \rangle_{\text{inside}}$ of the obese-class-I and obese-class-II male phantoms decreased by 17%–25% and 17%–40%, respectively, depending on the examination category. When comparing the obese-class-I and obese-class-III female phantoms to the normal-weight female phantom, the reduction in $\langle h \rangle_{\text{inside}}$ was 28%–42% and 51%–63%, respectively.

Table IX summarizes the effect of obesity when organ dose was normalized by SSDE. The $\langle h_{\text{ss}} \rangle_{\text{inside}}$ values of the obese-class-I and obese-class-II male phantoms agreed with those of the normal-weight male phantom to within 6% and 15%, respectively. However, relative to the normal-weight female phantom, the obese-class-I and obese-class-III female phantoms had $\langle h_{\text{ss}} \rangle_{\text{inside}}$ values lower by 20%–35% and 36%–49%, respectively. SSDE-normalized organ dose was not

TABLE VIII. Effect of obesity on $CTDI_{vol}$-to-organ dose conversion coefficients.

| | Scan length (cm)[b] | $\langle h \rangle_{inside}$ (unitless)[a] | | | | | |
|---|---|---|---|---|---|---|---|
| | | Male | | | Female | | |
| | | Normal | Obese class I | Obese class II | Normal | Obese class I | Obese class III |
| Chest-abdomen-pelvis | 71 ± 3 | 1.35 | 1.12 (−17%) | 0.89 (−34%) | 1.37 | 0.91 (−33%) | 0.64 (−54%) |
| Chest | 33 ± 3 | 1.44 | 1.16 (−19%) | 0.92 (−36%) | 1.48 | 1.00 (−33%) | 0.73 (−51%) |
| Abdomen-pelvis | 53 ± 2 | 1.27 | 1.04 (−18%) | 0.88 (−31%) | 1.26 | 0.80 (−37%) | 0.56 (−55%) |
| Abdomen | 31 ± 1 | 1.28 | 1.03 (−20%) | 0.79 (−38%) | 1.34 | 0.79 (−41%) | 0.57 (−58%) |
| Pelvis | 31 ± 1 | 1.13 | 0.93 (−18%) | 0.94 (−17%) | 1.03 | 0.75 (−28%) | 0.49 (−52%) |
| Adrenals | 15 ± 1 | 1.09 | 0.82 (−25%) | 0.65 (−40%) | 1.08 | 0.64 (−41%) | 0.44 (−59%) |
| Liver | 26 ± 2 | 1.25 | 1.00 (−20%) | 0.77 (−38%) | 1.32 | 0.76 (−42%) | 0.55 (−59%) |
| Kidneys | 19 ± 1 | 1.05 | 0.87 (−17%) | 0.66 (−37%) | 1.21 | 0.72 (−41%) | 0.45 (−63%) |
| Liver-to-kidney | 27 ± 2 | 1.23 | 1.01 (−18%) | 0.79 (−36%) | 1.30 | 0.78 (−40%) | 0.56 (−57%) |
| Kidney-to-bladder | 41 ± 1 | 1.13 | 0.89 (−21%) | 0.77 (−32%) | 1.20 | 0.74 (−38%) | 0.51 (−58%) |

[a]For given phantom and examination category, $\langle h \rangle_{inside}$ is the $CTDI_{vol}$-to-organ dose conversion coefficient averaged across fully encompassed organs (i.e., organs completely inside the scan coverage). Values in parenthesis are the percent differences between an obese phantom and the normal-weight phantom in the same gender category.
[b]Scan length = image coverage + over-ranging distance.

independent of patient diameter and generally decreased with increasing obesity level.

The effectiveness of SSDE as an estimator of organ dose was assessed using the percent difference between SSDE and average dose to fully encompassed organs (Table X). For the normal-weight male, normal-weight female, and obese-class-I male phantoms, the differences between SSDE and average dose to fully encompassed organs were less than 40%, thus less than the maximum dose variability of 47% across fully encompassed organs (Table V). However, this was not the case for the rest of the phantoms. The effectiveness of SSDE as an estimator of organ dose generally declined with increasing obesity level. Although the obese-class-I male and female phantoms had similar BMI, SSDE approximated organ dose of the former much better than the latter. The comparison between SSDE and average dose to fully encompassed organs is also illustrated in Fig. 2. Both dose quantities are normalized by $CTDI_{vol}$.

Relative to the normal-weight male phantom, $k$ factors of the obese-class-I and obese-class-II male phantoms decreased by 15%–30% and 14%–46%, respectively, depending on the examination category (Table VI). When comparing the obese-class-I and obese-class-III female phantoms to the normal-weight female phantom, the reduction in $k$ factor was 12%–40% and 44%–59%, respectively. Similar reduction with increasing obesity was also found for the $q$ factors (Table VII).

## IV. DISCUSSION

To promote the appropriate use of CT radiation and avoid unnecessary exposure, various institutions are developing

TABLE IX. Effect of obesity on SSDE-to-organ dose conversion coefficients.

| | Scan length (cm) | $\langle h_{ss} \rangle_{inside}$ (unitless)[a] | | | | | |
|---|---|---|---|---|---|---|---|
| | | Male | | | Female | | |
| | | Normal | Obese class I | Obese class II | Normal | Obese class I | Obese class III |
| Chest-abdomen-pelvis | 71 ± 3 | 0.96 | 0.97 (2%) | 0.85 (−11%) | 1.03 | 0.76 (−26%) | 0.64 (−38%) |
| Chest | 33 ± 3 | 1.04 | 1.03 (−1%) | 0.88 (−15%) | 1.11 | 0.83 (−26%) | 0.71 (−36%) |
| Abdomen-pelvis | 53 ± 2 | 0.89 | 0.90 (1%) | 0.84 (−5%) | 0.94 | 0.66 (−30%) | 0.57 (−39%) |
| Abdomen | 31 ± 1 | 0.87 | 0.90 (3%) | 0.78 (−10%) | 0.98 | 0.64 (−34%) | 0.57 (−42%) |
| Pelvis | 31 ± 1 | 0.81 | 0.79 (−3%) | 0.88 (8%) | 0.80 | 0.63 (−20%) | 0.51 (−36%) |
| Adrenals | 15 ± 1 | 0.74 | 0.72 (−3%) | 0.64 (−13%) | 0.78 | 0.52 (−34%) | 0.44 (−44%) |
| Liver | 26 ± 2 | 0.85 | 0.87 (3%) | 0.76 (−10%) | 0.96 | 0.62 (−35%) | 0.55 (−43%) |
| Kidneys | 19 ± 1 | 0.71 | 0.76 (6%) | 0.65 (−9%) | 0.88 | 0.58 (−34%) | 0.45 (−49%) |
| Liver-to-kidney | 27 ± 2 | 0.84 | 0.88 (5%) | 0.78 (−7%) | 0.94 | 0.63 (−33%) | 0.56 (−41%) |
| Kidney-to-bladder | 41 ± 1 | 0.79 | 0.77 (−3%) | 0.74 (−7%) | 0.90 | 0.62 (−31%) | 0.51 (−43%) |

[a]For given phantom and examination category, $\langle h_{ss} \rangle_{inside}$ is the SSDE-to-organ dose conversion coefficient averaged across fully encompassed organs (i.e., organs completely inside the scan coverage). Values in parenthesis are the percent differences between an obese phantom and the normal-weight phantom in the same gender category.

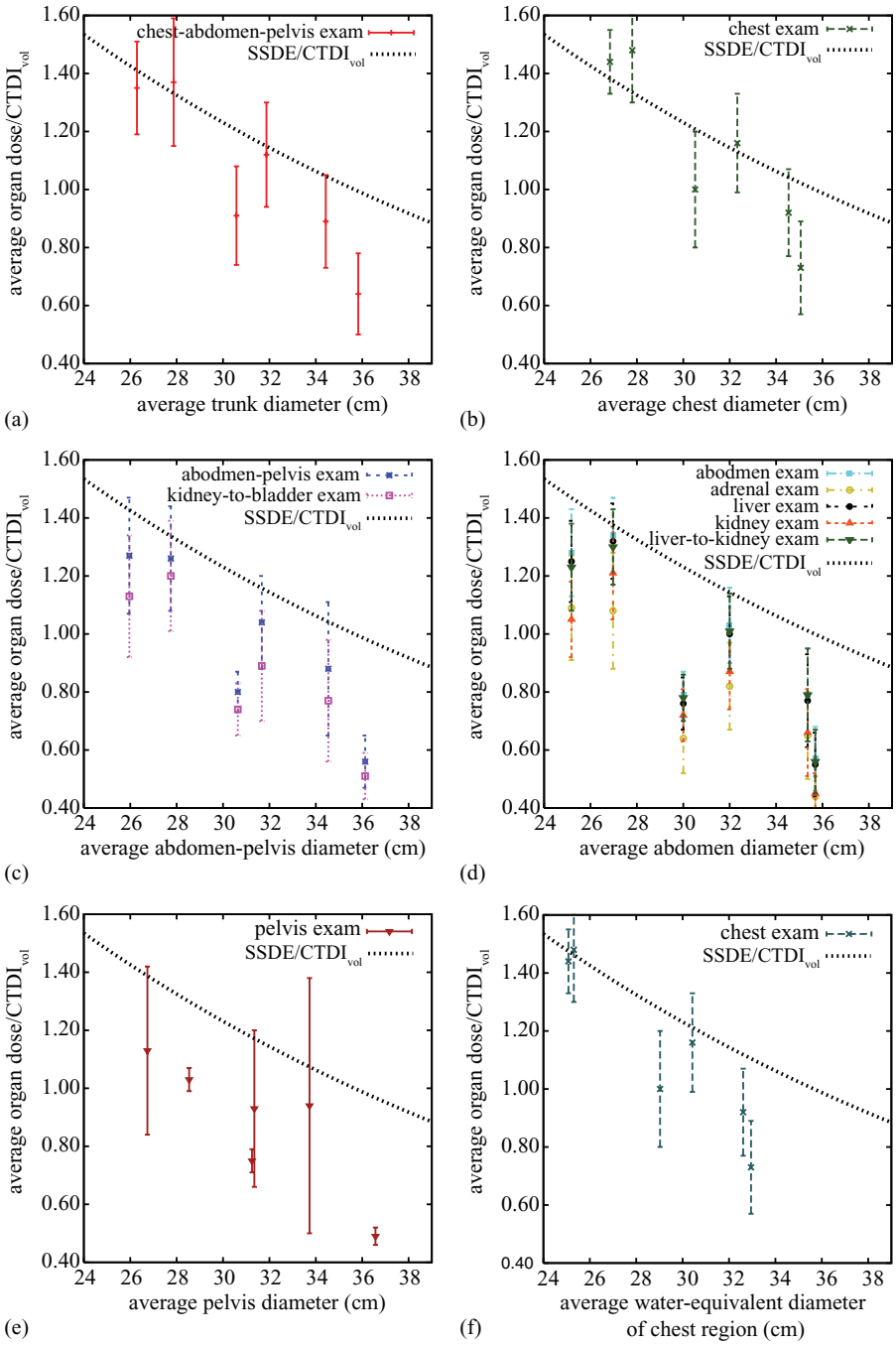


FIG. 2. Comparison between size-specific dose estimate (SSDE) and average dose to fully encompassed organs. Both dose quantities are normalized by $CTDI_{vol}$. The error bars correspond to standard deviations across fully encompassed organs. Average water-equivalent diameter of chest region was calculated assuming a mean beam energy of 83 keV.

software applications to automatically extract quality assurance dose quantities, namely $CTDI_{vol}$ and DLP.[31–33] To compare these dose quantities across different CT protocols in a meaningful way and to accumulate the dose information to yield a cumulative dose/risk profile for a given patient,[34] it is necessary to convert such quality assurance dose quantities into patient dose estimates and risk estimates. Dose and risk conversion coefficients provide a practical method for performing such conversions. In this study, we obtained $CTDI_{vol}$-to-organ-dose, SSDE-to-organ-dose, DLP-to-effective-dose, and DLP-to-risk-index conversion coefficients (denoted as $h$, $h_{ss}$, $k$, and $q$ factors, respectively) for a wide range of body CT protocols. We quantified their variability across examination categories and further evaluated the effect of obesity.

## IV.A. Effect of protocol

Our study showed that the $h$ factor for a given organ is similar among examination categories that cover the entire organ volume (the variability was generally less than 15%)

TABLE X. Effectiveness of SSDE as an estimator of average dose to fully encompassed organs[a].

| | Male | | | Female | | |
|---|---|---|---|---|---|---|
| | Normal (%) | Obese class I (%) | Obese class II (%) | Normal (%) | Obese class I (%) | Obese class III (%) |
| Chest-abdomen-pelvis | 5 | 3 | 18 | −3 | 32 | 56 |
| Chest | −4 | −3 | 13 | −10 | 21 | 40 |
| Abdomen-pelvis | 12 | 11 | 18 | 6 | 51 | 74 |
| Abdomen | 15 | 11 | 28 | 3 | 56 | 77 |
| Pelvis | 23 | 26 | 14 | 26 | 58 | 97 |
| Adrenals | 35 | 40 | 56 | 28 | 92 | 127 |
| Liver | 18 | 14 | 31 | 4 | 61 | 82 |
| Kidneys | 40 | 31 | 53 | 14 | 72 | 124 |
| Liver-to-kidney | 19 | 13 | 28 | 6 | 58 | 80 |
| Kidney-to-bladder | 26 | 30 | 35 | 11 | 61 | 95 |

[a]Percent value in the table equals $\frac{SSDE-\langle D\rangle_{\text{inside}}}{\langle D\rangle_{\text{inside}}} \times 100\% = (\frac{1}{\langle h_{ss}\rangle_{\text{inside}}} - 1) \times 100\%$, where $\langle D\rangle_{\text{inside}}$ denotes average dose to fully encompassed organs. $\langle h_{ss}\rangle_{\text{inside}}$ is the value reported in Table IX.

(Table IV). This can be explained by the fact that, for a fully encompassed organ, the dose difference between one examination category and another was mainly due to the difference in scattered radiation caused by the difference in scan coverage. The $h$ factor was generally greater for a longer scan length (Tables XII–XVII). The small variability of the $h$ factor across examination categories suggested the feasibility of estimating dose to fully encompassed organs from $CTDI_{vol}$ using protocol-independent conversion coefficients. For the same patient, the scan coverage may vary from an initial CT study to a follow-up CT study and may also vary from one hospital to another. However, the same $h$ factor can be used to estimate organ dose as long as the organ is entirely inside the scan coverage. In contrast to the variability across examination categories for the same organ, the variability across organs for the same examination category was higher (up to 47%) (Table V). This can be explained by the differences in the location, size, and spatial spread of the organs. $CTDI_{vol}$ represents a radial average of dose over the area of the central scan plan located at $z = 0$ for a 100-mm scan length. It ignores the radial location of the organ, the $z$-location of the organ relative to $z = 0$, and the actual scan length used clinically. The variability of $h$ factors across examination categories and organs reflect these inherent limitations of the $CTDI_{vol}$ concept.

Given the large number of radiosensitive organs exposed in a CT scan, estimating/tracking dose for all the radiosensitive organs can be cumbersome and even impractical for the purpose of radiation monitoring and protocol optimization. As such, effective dose (hence $k$ factor) has been widely used in the management of CT radiation. Our study showed that $k$ factor varies considerably across different examination categories in body CT (15%–27%) independent of obesity level. $k$ factors developed for the examination of the entire abdominopelvic region cannot be used to effectively substitute the $k$ factors for the examinations of a subregion (e.g., kidneys and adrenal glands). As such, a separate $k$ factor is needed for each examination category. This result can be understood from the definition of DLP, which is simply a measure of the total energy deposited and is indifferent to how the dose is distributed along the z-axis. Thus, predicting effective dose from DLP requires significant constraints on scan coverage.

Despite its simple and succinct nature, the validity of effective dose for medical procedures was recently under scrutiny.[29,35–38] As the tissue-weighting factors are mean values representing averages over both gender and age,[23] effective dose does not reflect the risk difference due to difference in age and gender. Furthermore, as explained in the ICRP Publication 103,[23] "The age distributions for workers

TABLE XI. Comparison between organ dose obtained in this study and organ dose predicted by published exponential relationships relating organ dose with patient diameter/perimeter.

| | Male | | | Female | | |
|---|---|---|---|---|---|---|
| | Normal | Obese class I | Obese class II | Normal | Obese class I | Obese class III |
| **Chest CT** | | | | | | |
| Average chest diameter (cm) | 26.8 | 32.3 | 34.5 | 27.8 | 30.5 | 35.1 |
| Lung dose simulated in this study (mGy/100 mAs) | 8.73 | 7.14 | 5.72 | 9.63 | 6.10 | 4.68 |
| Lung dose predicted using the equation of Li *et al.* (mGy/100 mAs)[a] | 9.49 | 7.83 | 7.25 | 9.18 | 8.35 | 7.12 |
| Discrepancy | 9% | 10% | 27% | −5% | 37% | 52% |
| **Abdominal CT** | | | | | | |
| Average abdominal diameter (cm) | 25.2 | 32.0 | 35.4 | 27.0 | 30.0 | 35.7 |
| Stomach dose estimated in this study (mGy/100 mAs) | 8.53 | 6.74 | 5.21 | 8.77 | 5.41 | 4.01 |
| Stomach dose predicted using the equation of Turner *et al.* (mGy/100 mAs)[b] | 9.29 | 7.29 | 6.47 | 8.72 | 7.83 | 6.40 |
| Discrepancy | 9% | 8% | 24% | −1% | 45% | 59% |

[a]The equation for lung dose and the set of scan parameters in this study is $H_{\text{lung}} = \exp(-0.035 d_{\text{chest}} + 3.19)$ in mGy/100 mAs. See supplementary materials of Li *et al.* (Ref. 7).

[b]The equation for stomach dose is $H_{\text{stomach}} = 3.780 \times \exp(-0.0113 \times \pi d_{\text{abomen-pelvis}}) \times CTDI_{vol}$. The $CTDI_{vol}$ for the set of scan parameters in this study was 6.01 mGy/100 mAs. See Turner *et al.* (Ref. 10).

and the general population (for which the effective dose is derived) can be quite different from the overall age distribution for the patients undergoing medical procedures using ionising radiation. The age distribution also differs from one type of medical procedure to another, depending on the prevalence of the individuals for the medical condition being evaluated."

To address the limitations of the effective dose concept, Brenner proposed an alternative quantity called "effective risk," which is the summation of cancer risks to individual organs.[28] By using gender-specific and age-specific risk coefficients, effective risk can be applied to any patient or patient cohort and has a straightforward interpretation. We recently applied the "effective risk" concept to CT dosimetry, but renamed this quantity "risk *index*,"[6] to acknowledge the large uncertainty associated with risk estimation in the low-dose range, particularly as it relates to individual patients, who might have variable radiosensitivity due to generic factors and hormonal profiles. In this study, we showed that the conversion coefficient from DLP to risk index ($q$ factor) varies slightly (<10%) for male patients, but considerably (21–43%) for female patients, across body examination categories. The large variability in female $q$ factor can be explained by the substantially higher risks of lung cancer and breast cancer as compared to other cancers (Fig. 3). The abdominal and pelvic examinations have similar scan length. However, lungs and breasts receive much higher dose in an abdominal examination. Although ovaries, uterus, and bladder receive much higher dose in a pelvic examination, their risks of cancer incidence are substantially lower than those of the lungs and the breasts. The net result is that the overall risk index, hence $q$ factor, is substantially lower in a pelvic examination. For male patients, the cancer risks of different organs do not exhibit such a large disparity (Fig. 3). These results suggest that in body CT, although a protocol-independent $q$ factor is feasible for male patients, it is not feasible for female patients.

### IV.B. Effect of obesity

Our study showed that $h$ factors generally decrease with increasing obesity level. This is consistent with earlier findings that, when the same scan technique is used, organ dose decreases with increasing patient size.[39,40] Recently, the effect of obesity on CT dose was explicitly studied by Ding *et al.* at Rensselaer Polytechnic Institute (RPI).[41] Ding *et al.* extended the RPI-adult male and female computational phantoms to reference obesity patients by adding subcutaneous adipose tissue (SAT) beneath the skin and by adjusting the density of the visceral adipose tissue (VAT) to account for the larger VAT masses expected for obese patients. They showed that in a chest-abdomen-pelvis CT scan, when the same scanner operating parameters were used, dose to colon, an organ deep in the abdomen was 59% lower for an obese-class-III female phantom (BMI: 46.4 kg/m$^2$) as compared to a normal-weight female phantom (BMI: 23.9 kg/m$^2$). While the obese phantoms in our study were created using a different approach (i.e., based on segmentations from clinical CT images), a similar result was obtained. For the chest-abdomen-pelvis examination in our study, $h$ factor for larger intestine was 51% lower for the obese-class-III female phantom (BMI: 42.0 kg/m$^2$) compared to the normal-weight female phantom (BMI: 24.5 kg/m$^2$) (Tables XV and XVII). Percent reduction in breast dose, however, differed substantially between our study (57%) and the study of Ding *et al.* (24%). This can be explained by the fact that going from normal-weight female phantom to obese-class-III female phantom, the change in chest diameter (at mid-chest) was substantially different in these two studies. In the study of Ding *et al.*, chest diameter (calculated from lateral and AP dimensions) increased from 27.9 cm in the normal-weight female phantom to 31.9 cm in the obese-class-III female phantom (referred to as morbidly obese phantom), whereas the corresponding change in our study was much greater, from 27.4 cm to 35.2 cm.

Recent studies have correlated $h$ factors (hence organ dose) with patient diameter.[7,10] Li *et al.* reported the exponential relationships between $h$ factors and patient chest diameter for pediatric chest CT, obtained using patient-specific computational phantoms of 30 pediatric patients.[7] For fully encompassed organs in abdominal CT, Turner *et al.* published the exponential relationships between $h$ factors and patient abdominal perimeter, obtained using the GSF family of voxelized phantoms, which includes body habitus from baby to overweight adult.[10] In Table XI, we compared the dose results of the present study with the dose predicted by these published exponential relationships. Extrapolation was needed since the study by Li *et al.* was limited to the pediatric population (maximum average chest diameter of 23 cm) while the study by Turner *et al.* was limited to a patient diameter of 33.8 cm (perimeter of 106.2 cm). Lung dose in chest CT and stomach dose in abdomen-pelvis CT were used for the comparison. The published relationships predicted dose to fully encompassed organs very well for the normal-weight phantoms and the obese-class-I male phantom. However, they severely overestimated the organ dose for the more obese phantoms. The overestimation can only be partially explained by the need for extrapolation. For abdominal CT examination of the two obese-class-I phantoms, extrapolation was not needed since their abdominal diameters were within the range of diameters

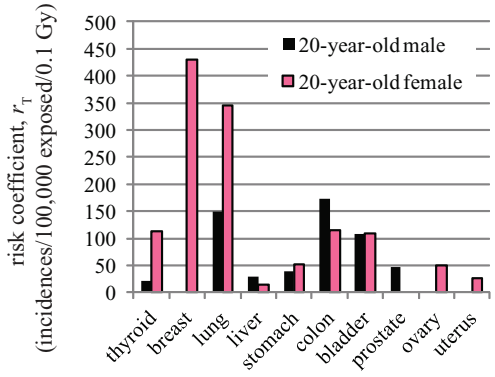


FIG. 3. Risk coefficients (cancer incidences per 100 000 persons exposed to a single dose of 0.1 Gy) tabulated in BEIR VII report (Ref. 29).

investigated by Turner *et al.* However, the predicted stomach dose was accurate for the male phantom, but very inaccurate for the female phantom. This result can be best explained by the difference in organ size and fat distribution between these two phantoms (Fig. 1). The thick subcutaneous fat (modeled as soft tissue) in the female phantom provided "radiation shielding" for her internal organs. The above analysis indicates that organ dose cannot be accurately predicted using patient diameter alone. The variability in organ locations due to variable fat distributions must also be taken into consideration. This result together with the discrepancy between our study and the study of Ding *et al.* suggest the need for a large-scale study to include the entire ranges of patient sizes and different types of fat distributions to identify and fully characterize various influencing factors and the uncertainties they introduce into organ dose estimation.

Another finding of our study was that for obese phantoms the differences between SSDE and average dose to fully encompassed organs generally exceed the dose variability across such organs (Table X and Fig. 2). SSDE generally overestimates organ dose for obese patients. This may be understood by the fact that the organs of obese patients are more centrally located (Fig. 1), the average dose of which is lower than the average dose across the entire cross-sectional area as represented by SSDE by its definition. For this reason, SSDE-normalized organ dose is also not independent of patient diameter.

In AAPM Report No. 204, the functional dependence of the ratio SSDE/$\text{CTDI}_{\text{vol}}$ on effective diameter was a result of curve fitting to data generated by four research groups. Two of the groups determined effective diameters as water-equivalent diameters. The other two groups determined effective diameters as physical (geometric) diameters. Table XVIII summarizes both types of diameters for the different body regions of the six phantoms in this study. Physical diameters, $d$, were calculated using Eq. (4). Water-equivalent diameters, $d_{\text{w}}$, were calculated as

$$d_w = 2\sqrt{\frac{\langle A_w \rangle_{\text{region}}}{\pi}}, \tag{5}$$

where $A_w$ is the water-equivalent area of a single axial slice in the phantom and $\langle A_w \rangle_{\text{region}}$ is the average of $A_w$ over all the axial slices in a given body region. $A_w$ was calculated as

$$A_w = A \cdot \left\langle \frac{\mu^{\bar{E}}_{\text{voxel}}}{\mu^{\bar{E}}_{\text{water}}} \right\rangle, \tag{6}$$

where $A$ is the physical cross-sectional area of the axial slice and $\langle \frac{\mu^{\bar{E}}_{\text{voxel}}}{\mu^{\bar{E}}_{\text{water}}} \rangle$ is the attenuation coefficient ratio between the voxel material (i.e., soft tissue, lung, breast, and average skeleton) and water calculated at the mean energy of the CT beam, $\bar{E}$, and averaged over all the voxels in the axial slice. This method of water-equivalent diameter calculation is equivalent to the method reported by Menke[42] and Huda *et al.*[43,44] In those earlier studies, water-equivalent diameters were calculated from clinical CT images of patients, where $\langle \frac{\mu^{\bar{E}}_{\text{voxel}}}{\mu^{\bar{E}}_{\text{water}}} \rangle = \frac{\langle \text{CT} \rangle}{1000} + 1$ with $\langle \text{CT} \rangle$ being the mean CT number of an axial CT slice. Due to beam hardening, the mean energy of the CT beam, $\bar{E}$, varies from patient to patient and from voxel to voxel, depending on patient size and surrounding tissues. This variation of $\bar{E}$ with patient size and voxel location is partially taken into account when $d_w$ is calculated from clinical CT images because no beam-hardening correction algorithm fully corrects beam-hardening artifact present in an image.[45] In this study, we ignored the variation of $\bar{E}$ with patient size and voxel location, but calculated $d_w$ using two extreme $\bar{E}$ values, 62 keV and 83 keV, to assess how beam hardening affects the estimates of $d_w$. The first value is the mean energy of the 120 kVp beam at the isocenter of the GE LightSpeed VCT scanner. It was calculated after attenuating the prebowtie spectrum (at the exit of the x-ray tube and before filtration by the bowtie filter) of the 120 kVp beam by the least attenuating section of the bowtie filter (at beam angle of 0°). The accuracy of the prebowtie spectrum has been validated in our previous study.[24] The second value was calculated after attenuating the prebowtie spectrum by 40 cm of water (representing an obese patient) and the most attenuating section of the bowtie filter (at beam angle of $\sim 27.5°$). Table XVIII shows that the differences between $d_w^{62\ \text{keV}}$ and $d_w^{83\ \text{keV}}$ were small (<1%), i.e., the effect of beam hardening on the estimates of $d_w$ was small. At either energy, the maximum discrepancies between $d_{\text{w}}$ and the physical diameter $d$ existed for chest and pelvis regions. Even for these regions, the differences between $d_{\text{w}}$ and $d$ were less than 9%, corresponding to SSDE differences of less than 10%. In Fig. 2(f), we also compared average dose to fully encompassed organs in the chest examination with SSDE calculated from water-equivalent diameters (at 83 keV). These results showed that using water-equivalent diameters does not significantly improve the effectiveness of SSDE as an estimator of organ dose.

The effect of patient size on $k$ factor has been studied in the past, resulting in the development of age-dependent $k$ factors (0, 1, 5, 10 years, and adult).[8,11] In this study, we showed sizable differences in $k$ and $q$ factors between adult phantoms of different obesity levels. This highlights the need to develop size-specific $k$ and $q$ factors for the entire spectrum of pediatric and adult body habitus.

It should be noted that while $h$, $k$, and $q$ factors generally decrease with increasing patient size, the scan techniques used for larger patients are generally higher. Therefore, the absolute dose and risk to larger patients may not be lower. Ding and coauthors showed that in a chest-abdomen-pelvis scan, when the mAs was doubled for the obese-class-I, obese-class-II, and obese-class-III phantoms, the absolute effective dose relative to that of the normal-weight phantom increased by 57%, 42%, and 23%, respectively.[41]

### IV.C. Necessity of whole-body dosimetry

It has been proposed that organ dose in a CT scan can be estimated in real time by incorporating an analytical or Monte Carlo simulation engine during or after the image reconstruction process. Several CT manufactures are devising methods to enable automatic organ segmentation. While this approach obviates the need to create whole-body

computational phantoms, it does not provide dose estimates for organs partially or completely invisible in the image volume. It may be argued that such organs do not contribute significantly to overall dose and risk estimates. With the organ dose data in Tables XII–XVII, we tested the validity of this argument. The organs in Tables XII–XVII were divided into four categories: inside (fully inside of the scan coverage), peripheral (on the periphery of the scan coverage), distributed (extended beyond the scan coverage on both ends, e.g., red marrow and muscle), and outside (fully outside of the scan coverage). The contributions to effective dose (hence $k$ factor) and risk index (hence $q$ factor) of the four organ categories are summarized in Tables XIX and XX. On average, inside, peripheral, distributed, and outside organs contributed 50% ± 19%, 38% ± 20%, 10% ± 3%, and 2% ± 1% to effective dose, respectively. The respective contributions to risk index were 46% ± 24%, 45% ± 24%, 8% ± 3%, and 2% ± 1%, i.e., peripheral organs had nearly identical contribution to risk index as inside organs. It should be noted that our definition of inside organs included those that were fully inside of the scan coverage (= image coverage + over-ranging distance), but partially outside of the image coverage. Therefore, the contributions to effective dose and risk index of fully imaged organs were even smaller than 50% ± 19% and 46% ± 24%, respectively. This result demonstrates the necessity of whole-body dosimetry and highlights the severe limitation of dose and risk estimations based on organs in the CT image volume only.

### IV.D. Limitations and future work

Our study has several limitations. First, the sample size of the study was small, and the phantoms may not represent the average patients in each obese class. However, the variability of $h$, $k$, and $q$ factors across examination categories is consistent across phantoms of vastly different body habitus. Thus, we do not expect the results to differ should more phantoms have been included in the study. While the phantoms in our study may not represent the anatomical average of the obesity classes they belong to, the reductions in $h$, $k$, and $q$ factors from one obesity class to another are indicative of the magnitude of the effects obesity has on these conversion coefficients. They highlight the need to conduct larger-scale dosimetry studies to encompass the full range of patient sizes and obesity levels. Efforts are currently underway at our institution to create a population of hundreds of computational phantoms from clinical CT images of patients. The effect of obesity will be more systematically investigated in future studies. Second, the concept of effective dose should in principle be applied to reference phantoms only.[23] Our application of the effective dose concept to patient-specific phantoms, while not being exactly as defined by ICRP, is in line with other studies in the literature.[40] Since the variability of the conversion coefficients across examination categories was consistent for phantoms of different obesity levels, we expect the finding to hold true for reference phantoms. Lastly, our study did not explicitly model the effect of tube current modulation (TCM). In a TCM scan, the variability of $h$ factor across examination categories is likely to increase. Since the mA-modulation profile is based on patient attenuation, it is reasonable to assume that for a given noise index a chest examination and a chest-abdomen-pelvis examination have the same mA-modulation profile for the chest part of the body. Thus, dose to chest organs would be similar in these two categories of examinations. However, the average $CTDI_{vol}$ of these two types of examinations may differ, depending on the mA-modulation profile for the abdomen-pelvis part of the body. Thus, between the two categories of examinations, the $h$ factors for the chest organs may differ more than they do in a fixed-mA examination. However, the increased variability due to mA-modulation may be reduced if the $CTDI_{vol}$ computed using a *local* average mA value (e.g., the average mA value for the image slices containing the organ) is used to normalize organ dose, in place of the $CTDI_{vol}$ computed using the average mA over the *entire* scan length, which is the value currently reported by the scanners based on the recommendation of the International Electrotechnical Commission (IEC). This is supported by our preliminary study of the effect of tube current modulation,[46] which showed that $h$ factors derived from fixed-mA examinations are a good approximation to those in TCM examinations if the $CTDI_{vol}$ computed using a *local* average mA value at the location of the organ is used to calculate the $h$ factor.

## V. CONCLUSIONS

In adult body CT, absorbed dose to a fully encompassed organ can be estimated from $CTDI_{vol}$ using a protocol-independent conversion coefficient. However, on average, fully encompassed organs only account for 50% ± 19% of $k$ factor and 46% ± 24% of $q$ factor. The dose received by partially encompassed and nonencompassed organs should not be neglected. To estimate effective dose and risk index from DLP, it is necessary to use conversion coefficients specific to the anatomical region examined. Obesity has a significant effect on dose and risk conversion coefficients, which cannot be predicted using body diameter alone. SSDE-normalized organ dose is not independent of patient diameter. SSDE itself generally overestimates organ dose for obese patients.

## ACKNOWLEDGMENTS

The authors thankfully acknowledge the supports from the Radiological Society of North America (Grant No. RR1141) and the National Institutes of Health (NIH) (Grant No. R01 EB001838-06).

## APPENDIX: ADDITIONAL DATA TABLES

See Tables XII–XX.

TABLE XII. $CTDI_{vol}$-to-organ dose conversion coefficients (*h* factors, unitless) for the **normal-weight male phantom**. The simulations were performed for the LightSpeed VCT scanner using a tube voltage of 120 kVp, a pitch of 1.375, a beam collimation of 40 mm, and large body scan field-of-view. $CTDI_{vol} = 6.01$ mGy/100 mAs. The *h* factors are in boldface for organs entirely inside the scan coverage.

| | Chest-abdomen-pelvis | Chest | Abdomen-pelvis | Abdomen | Pelvis | Adrenals | Liver | Kidneys | Liver-to-kidney | Kidney-to-bladder | COV[a] |
|---|---|---|---|---|---|---|---|---|---|---|---|
| Eyes | 0.01 | 0.02 | 0.001 | 0.001 | 0.0001 | 0.0004 | 0.001 | 0.0003 | 0.001 | 0.0005 | – |
| Brain | 0.02 | 0.02 | 0.001 | 0.001 | 0.0001 | 0.0005 | 0.001 | 0.0004 | 0.001 | 0.001 | – |
| Pharynx-larynx | 0.50 | 0.50 | 0.01 | 0.01 | 0.0003 | 0.004 | 0.01 | 0.004 | 0.01 | 0.004 | – |
| Thyroid | 1.21 | 1.21 | 0.02 | 0.02 | 0.0005 | 0.01 | 0.02 | 0.01 | 0.02 | 0.01 | – |
| Trachea-bronchi | **1.44** | **1.42** | 0.29 | 0.29 | 0.004 | 0.08 | 0.29 | 0.07 | 0.29 | 0.07 | **1%** |
| Breasts | **1.55** | **1.54** | 0.13 | 0.13 | 0.002 | 0.04 | 0.13 | 0.03 | 0.13 | 0.03 | **0.3%** |
| Thymus | **1.55** | **1.53** | 0.22 | 0.21 | 0.003 | 0.07 | 0.21 | 0.06 | 0.21 | 0.06 | **0.7%** |
| Esophagus | **1.28** | **1.24** | 0.49 | 0.49 | 0.01 | 0.23 | 0.49 | 0.19 | 0.49 | 0.20 | **2%** |
| Lungs | **1.49** | **1.45** | 0.59 | 0.59 | 0.01 | 0.21 | 0.58 | 0.17 | 0.58 | 0.17 | **2%** |
| Heart | **1.51** | **1.46** | 1.03 | 1.03 | 0.01 | 0.37 | 1.02 | 0.27 | 1.02 | 0.28 | **2%** |
| Liver | **1.35** | 1.09 | **1.24** | **1.23** | 0.04 | 0.93 | **1.21** | 0.92 | **1.21** | 0.96 | **5%** |
| Gall bladder | **1.37** | 0.73 | **1.50** | **1.49** | 0.08 | **1.26** | **1.45** | **1.21** | **1.44** | **1.28** | **8%** |
| Spleen | **1.37** | 1.03 | **1.31** | **1.30** | 0.04 | **1.10** | **1.29** | 1.10 | **1.27** | 1.14 | **7%** |
| Stomach | **1.48** | 1.19 | **1.42** | **1.41** | 0.05 | **1.17** | **1.40** | 1.14 | **1.38** | 1.18 | **8%** |
| Pancreas | **1.29** | 0.87 | **1.23** | **1.22** | 0.07 | 0.98 | **1.19** | **1.03** | **1.18** | **1.08** | **8%** |
| Adrenal glands | **1.13** | 0.83 | **1.05** | **1.04** | 0.05 | **0.84** | **1.02** | **0.90** | **1.01** | **0.94** | **9%** |
| Kidneys | **1.27** | 0.45 | **1.24** | **1.23** | 0.12 | 0.87 | **1.17** | **1.07** | **1.14** | **1.17** | **6%** |
| Large intestine | **1.39** | 0.17 | **1.39** | 0.99 | 0.77 | 0.39 | 0.71 | 0.65 | 0.68 | **1.35** | **2%** |
| Small intestine | **1.46** | 0.28 | **1.43** | 1.18 | 0.73 | 0.50 | 0.89 | 0.75 | 0.83 | **1.41** | **2%** |
| Prostate | **0.92** | 0.002 | **0.93** | 0.04 | **0.91** | 0.003 | 0.01 | 0.01 | 0.01 | **0.79** | **7%** |
| Bladder | **1.20** | 0.002 | **0.99** | 0.05 | **1.03** | 0.004 | 0.02 | 0.01 | 0.01 | **1.05** | **8%** |
| Testes | **1.22** | 0.001 | **1.53** | 0.01 | **1.46** | 0.001 | 0.003 | 0.002 | 0.002 | 0.35 | **11%** |
| Residual soft tissues | 0.62 | 0.23 | 0.46 | 0.22 | 0.32 | 0.08 | 0.17 | 0.12 | 0.15 | 0.36 | – |
| Bone surface | 1.28 | 0.64 | 0.86 | 0.49 | 0.52 | 0.19 | 0.36 | 0.24 | 0.35 | 0.70 | – |
| Red bone marrow | 0.84 | 0.42 | 0.59 | 0.36 | 0.34 | 0.14 | 0.27 | 0.18 | 0.26 | 0.48 | – |
| Skin | 0.39 | 0.21 | 0.28 | 0.22 | 0.11 | 0.09 | 0.18 | 0.12 | 0.17 | 0.22 | – |
| COV[b] | **12%** | **8%** | **16%** | **11%** | **26%** | **16%** | **12%** | **12%** | **12%** | **18%** | – |

[a]Coefficient of variation (standard deviation × 100%/mean) across examination categories that covered the entire organ volume.
[b]Coefficient of variation (standard deviation × 100%/mean) across organs entirely inside the scan coverage.

TABLE XIII. $CTDI_{vol}$-to-organ dose conversion coefficients (*h* factors, unitless) for the **obese-class-I male phantom**. The simulations were performed for the LightSpeed VCT scanner using a tube voltage of 120 kVp, a pitch of 1.375, a beam collimation of 40 mm, and large body scan field-of-view. $CTDI_{vol} = 6.01$ mGy/100 mAs. The *h* factors are in boldface for organs entirely inside the scan coverage.

| | Chest-abdomen-pelvis | Chest | Abdomen-pelvis | Abdomen | Pelvis | Adrenals | Liver | Kidneys | Liver-to-kidney | Kidney-to-bladder | COV[a] |
|---|---|---|---|---|---|---|---|---|---|---|---|
| Eyes | 0.02 | 0.02 | 0.001 | 0.001 | 0.00003 | 0.0004 | 0.001 | 0.0004 | 0.001 | 0.0003 | – |
| Brain | 0.02 | 0.02 | 0.001 | 0.001 | 0.0001 | 0.0005 | 0.001 | 0.0004 | 0.001 | 0.0005 | – |
| Pharynx-larynx | 0.44 | 0.44 | 0.02 | 0.02 | 0.0004 | 0.006 | 0.02 | 0.005 | 0.02 | 0.005 | – |
| Thyroid | 0.86 | 0.85 | 0.03 | 0.03 | 0.0007 | 0.01 | 0.03 | 0.01 | 0.03 | 0.01 | – |
| Trachea-bronchi | **1.10** | **1.08** | 0.26 | 0.26 | 0.004 | 0.06 | 0.26 | 0.05 | 0.26 | 0.06 | **1%** |
| Breasts | **1.42** | **1.41** | 0.34 | 0.34 | 0.002 | 0.04 | 0.34 | 0.03 | 0.34 | 0.03 | **0.6%** |
| Thymus | **1.31** | **1.31** | 0.23 | 0.23 | 0.002 | 0.05 | 0.22 | 0.04 | 0.23 | 0.04 | **0.4%** |
| Esophagus | **0.98** | **0.93** | 0.46 | 0.45 | 0.01 | 0.18 | 0.45 | 0.16 | 0.45 | 0.16 | **3%** |
| Lungs | **1.22** | **1.19** | 0.55 | 0.55 | 0.01 | 0.14 | 0.54 | 0.12 | 0.54 | 0.12 | **2%** |
| Heart | **1.26** | **1.21** | 0.91 | 0.91 | 0.01 | 0.26 | 0.91 | 0.20 | 0.91 | 0.21 | **3%** |
| Liver | **1.12** | 0.89 | **1.03** | **1.02** | 0.04 | 0.73 | **1.00** | 0.72 | **1.01** | 0.74 | **4%** |
| Gall bladder | **1.29** | 0.92 | **1.26** | **1.25** | 0.07 | **0.99** | **1.22** | **1.07** | **1.23** | **1.11** | **9%** |
| Spleen | **1.15** | **1.00** | **1.05** | **1.05** | 0.03 | 0.82 | **1.04** | 0.80 | **1.04** | 0.81 | **5%** |
| Stomach | **1.16** | 0.84 | **1.12** | **1.11** | 0.06 | **0.88** | **1.09** | **0.90** | **1.10** | **0.92** | **11%** |
| Pancreas | **0.98** | 0.53 | **0.95** | **0.92** | 0.11 | **0.72** | **0.88** | **0.80** | **0.90** | **0.85** | **9%** |

TABLE XIII. (*Continued*)

| | Chest-abdomen-pelvis | Chest | Abdomen-pelvis | Abdomen | Pelvis | Adrenals | Liver | Kidneys | Liver-to-kidney | Kidney-to-bladder | COV[a] |
|---|---|---|---|---|---|---|---|---|---|---|---|
| Adrenal glands | **0.93** | 0.61 | **0.87** | **0.86** | 0.07 | **0.67** | **0.83** | **0.72** | **0.84** | **0.75** | **11%** |
| Kidneys | **1.02** | 0.29 | **1.01** | **0.98** | 0.18 | 0.74 | **0.92** | **0.88** | **0.93** | **0.96** | **5%** |
| Large intestine | **1.22** | 0.17 | **1.23** | 0.84 | 0.69 | 0.41 | 0.64 | 0.64 | 0.71 | 1.19 | **1%** |
| Small intestine | **1.21** | 0.13 | **1.20** | 0.88 | 0.75 | 0.35 | 0.59 | 0.68 | 0.71 | **1.17** | **2%** |
| Prostate | **0.70** | 0.001 | **0.72** | 0.02 | **0.71** | 0.003 | 0.01 | 0.01 | 0.01 | **0.59** | **9%** |
| Bladder | **0.83** | 0.002 | **0.88** | 0.03 | **0.86** | 0.005 | 0.01 | 0.01 | 0.02 | **0.75** | **7%** |
| Testes | **1.28** | 0.0003 | **1.13** | 0.01 | **1.23** | 0.001 | 0.002 | 0.003 | 0.003 | 0.20 | **6%** |
| Residual soft tissues | 0.58 | 0.22 | 0.45 | 0.23 | 0.29 | 0.10 | 0.18 | 0.14 | 0.19 | 0.35 | – |
| Bone surface | 1.11 | 0.60 | 0.75 | 0.43 | 0.43 | 0.18 | 0.35 | 0.22 | 0.35 | 0.57 | – |
| Red bone marrow | 0.67 | 0.34 | 0.47 | 0.28 | 0.27 | 0.12 | 0.23 | 0.15 | 0.23 | 0.37 | – |
| Skin | 0.37 | 0.20 | 0.27 | 0.21 | 0.12 | 0.10 | 0.17 | 0.12 | 0.18 | 0.21 | – |
| COV[b] | **16%** | **15%** | **16%** | **13%** | **28%** | **18%** | **13%** | **15%** | **13%** | **22%** | – |

[a]Coefficient of variation (standard deviation × 100% / mean) across examination categories that covered the entire organ volume.
[b]Coefficient of variation (standard deviation × 100% / mean) across organs entirely inside the scan coverage.

TABLE XIV. $CTDI_{vol}$-to-organ dose conversion coefficients (*h* factors, unitless) for the **obese-class-II male phantom**. The simulations were performed for the LightSpeed VCT scanner using a tube voltage of 120 kVp, a pitch of 1.375, a beam collimation of 40 mm, and large body scan field-of-view. $CTDI_{vol} = 6.01$ mGy/100 mAs. The *h* factors are in boldface for organs entirely inside the scan coverage.

| | Chest-abdomen-pelvis | Chest | Abdomen-pelvis | Abdomen | Pelvis | Adrenals | Liver | Kidneys | Liver-to-kidney | Kidney-to-bladder | COV[a] |
|---|---|---|---|---|---|---|---|---|---|---|---|
| Eyes | 0.02 | 0.02 | 0.001 | 0.001 | 0.00003 | 0.0003 | 0.001 | 0.0003 | 0.001 | 0.0003 | – |
| Brain | 0.02 | 0.02 | 0.001 | 0.001 | 0.0001 | 0.0003 | 0.001 | 0.0003 | 0.001 | 0.0003 | – |
| Pharynx-larynx | 0.51 | 0.50 | 0.01 | 0.01 | 0.0004 | 0.005 | 0.01 | 0.004 | 0.01 | 0.004 | – |
| Thyroid | 0.78 | 0.78 | 0.02 | 0.02 | 0.0006 | 0.01 | 0.02 | 0.01 | 0.02 | 0.01 | – |
| Trachea-bronchi | **0.89** | **0.88** | 0.18 | 0.18 | 0.004 | 0.05 | 0.18 | 0.04 | 0.18 | 0.04 | **1%** |
| Breasts | **0.79** | **0.78** | 0.67 | 0.67 | 0.003 | 0.05 | 0.67 | 0.03 | 0.67 | 0.04 | **0.7%** |
| Thymus | **1.13** | **1.12** | 0.13 | 0.13 | 0.002 | 0.04 | 0.13 | 0.03 | 0.13 | 0.03 | **0.8%** |
| Esophagus | **0.78** | **0.75** | 0.30 | 0.30 | 0.01 | 0.11 | 0.30 | 0.08 | 0.30 | 0.08 | **3%** |
| Lungs | **0.99** | **0.95** | 0.42 | 0.42 | 0.01 | 0.13 | 0.42 | 0.09 | 0.42 | 0.09 | **2%** |
| Heart | **1.09** | **1.06** | 0.54 | 0.54 | 0.01 | 0.12 | 0.54 | 0.09 | 0.54 | 0.09 | **2%** |
| Liver | **0.90** | 0.67 | **0.82** | **0.81** | 0.05 | 0.58 | **0.80** | 0.52 | **0.81** | 0.53 | **5%** |
| Gall bladder | **0.99** | 0.44 | **1.11** | **1.10** | 0.10 | **0.87** | **1.07** | **0.88** | **1.09** | **0.90** | **11%** |
| Spleen | **0.86** | 0.56 | **0.78** | **0.77** | 0.05 | **0.66** | **0.76** | 0.64 | **0.77** | 0.65 | **8%** |
| Stomach | **0.95** | 0.70 | **0.87** | **0.86** | 0.08 | **0.67** | **0.84** | 0.66 | **0.85** | 0.68 | **11%** |
| Pancreas | **0.78** | 0.31 | **0.75** | **0.72** | 0.18 | **0.54** | **0.68** | **0.63** | **0.71** | **0.67** | **11%** |
| Adrenal glands | **0.66** | 0.34 | **0.63** | **0.61** | 0.09 | **0.49** | **0.59** | **0.51** | **0.60** | **0.54** | **10%** |
| Kidneys | **0.76** | 0.15 | **0.74** | **0.70** | 0.24 | 0.54 | **0.66** | **0.64** | **0.68** | **0.70** | **6%** |
| Large intestine | **1.08** | 0.13 | **1.07** | 0.70 | 0.68 | 0.41 | 0.56 | 0.60 | 0.65 | **1.05** | **2%** |
| Small intestine | **1.05** | 0.08 | **1.05** | 0.73 | 0.80 | 0.28 | 0.49 | 0.60 | 0.65 | **1.03** | **1%** |
| Prostate | **0.58** | 0.001 | **0.59** | 0.02 | **0.58** | 0.004 | 0.01 | 0.01 | 0.01 | **0.51** | **6%** |
| Bladder | **0.75** | 0.002 | **0.77** | 0.03 | **0.79** | 0.007 | 0.01 | 0.02 | 0.02 | **0.75** | **2%** |
| Testes | **1.01** | 0.0005 | **1.39** | 0.01 | **1.44** | 0.002 | 0.004 | 0.006 | 0.007 | 1.04 | **18%** |
| Residual soft tissues | 0.46 | 0.19 | 0.35 | 0.18 | 0.22 | 0.10 | 0.16 | 0.12 | 0.17 | 0.28 | – |
| Bone surface | 0.87 | 0.50 | 0.54 | 0.29 | 0.32 | 0.13 | 0.25 | 0.16 | 0.26 | 0.41 | – |
| Red bone marrow | 0.51 | 0.27 | 0.33 | 0.18 | 0.20 | 0.08 | 0.16 | 0.10 | 0.16 | 0.26 | – |
| Skin | 0.30 | 0.16 | 0.22 | 0.16 | 0.10 | 0.09 | 0.15 | 0.11 | 0.15 | 0.17 | – |
| COV[b] | **18%** | **16%** | **26%** | **20%** | **47%** | **22%** | **21%** | **23%** | **20%** | **27%** | – |

[a]Coefficient of variation (standard deviation × 100%/mean) across examination categories that covered the entire organ volume.
[b]Coefficient of variation (standard deviation × 100%/mean) across organs entirely inside the scan coverage.

TABLE XV. $CTDI_{vol}$-to-organ dose conversion coefficients (*h* factors, unitless) for the **normal-weight female phantom**. The simulations were performed for the LightSpeed VCT scanner using a tube voltage of 120 kVp, a pitch of 1.375, a beam collimation of 40 mm, and large body scan field-of-view. $CTDI_{vol}$ = 6.01 mGy/100 mAs. The *h* factors are in boldface for organs entirely inside the scan coverage.

| | Chest-abdomen-pelvis | Chest | Abdomen-pelvis | Abdomen | Pelvis | Adrenals | Liver | Kidneys | Liver to kidneys | Kidneys to bladder | COV[a] |
|---|---|---|---|---|---|---|---|---|---|---|---|
| Eyes | 0.02 | 0.02 | 0.001 | 0.001 | 0.00004 | 0.001 | 0.002 | 0.0004 | 0.002 | 0.001 | – |
| Brain | 0.03 | 0.03 | 0.001 | 0.001 | 0.00005 | 0.001 | 0.001 | 0.0004 | 0.001 | 0.0005 | – |
| Pharynx-larynx | 0.76 | 0.76 | 0.01 | 0.01 | 0.0003 | 0.01 | 0.01 | 0.01 | 0.01 | 0.01 | – |
| Thyroid | 1.49 | 1.49 | 0.03 | 0.03 | 0.001 | 0.02 | 0.03 | 0.01 | 0.03 | 0.01 | – |
| Trachea-bronchi | **1.53** | **1.52** | 0.28 | 0.28 | 0.003 | 0.11 | 0.28 | 0.07 | 0.28 | 0.07 | **1%** |
| Breasts | **1.37** | **1.36** | 0.39 | 0.39 | 0.002 | 0.13 | 0.39 | 0.06 | 0.39 | 0.06 | **0.5%** |
| Thymus | **1.73** | **1.72** | 0.35 | 0.35 | 0.003 | 0.13 | 0.35 | 0.08 | 0.35 | 0.08 | **0.5%** |
| Esophagus | **1.32** | **1.29** | 0.41 | 0.41 | 0.005 | 0.20 | 0.41 | 0.12 | 0.41 | 0.12 | **1%** |
| Lungs | **1.64** | **1.60** | 0.68 | 0.68 | 0.01 | 0.35 | 0.68 | 0.23 | 0.68 | 0.23 | **2%** |
| Heart | **1.65** | **1.61** | 1.26 | 1.26 | 0.01 | 0.68 | 1.25 | 0.40 | 1.25 | 0.40 | **2%** |
| Liver | **1.50** | 0.95 | **1.43** | **1.42** | 0.09 | 1.22 | **1.40** | 1.16 | **1.39** | 1.20 | **3%** |
| Gall bladder | **1.64** | 0.25 | **1.55** | **1.51** | 0.24 | 1.20 | **1.49** | **1.47** | **1.44** | **1.57** | **4%** |
| Spleen | **1.46** | **1.26** | **1.39** | **1.38** | 0.05 | **1.22** | **1.37** | **1.21** | **1.36** | **1.23** | **7%** |
| Stomach | **1.51** | 0.85 | **1.46** | **1.44** | 0.22 | 1.09 | **1.41** | **1.28** | **1.39** | **1.34** | **5%** |
| Pancreas | **1.29** | 0.58 | **1.26** | **1.24** | 0.19 | 0.95 | **1.21** | **1.12** | **1.18** | **1.19** | **5%** |
| Adrenal glands | **1.23** | 0.89 | **1.12** | **1.12** | 0.07 | **0.94** | **1.11** | **0.99** | **1.10** | **1.02** | **9%** |
| Kidneys | **1.34** | 0.50 | **1.31** | **1.29** | 0.16 | 1.04 | **1.27** | **1.18** | **1.25** | **1.25** | **4%** |
| Large intestine | **1.32** | 0.10 | **1.29** | 0.83 | 0.91 | 0.29 | 0.71 | 0.59 | 0.57 | **1.28** | **2%** |
| Small intestine | **1.38** | 0.09 | **1.36** | 1.01 | 0.96 | 0.29 | 0.86 | 0.70 | 0.63 | **1.36** | **1%** |
| Ovaries | **1.01** | 0.004 | **1.08** | 0.10 | **1.05** | 0.01 | 0.06 | 0.04 | 0.04 | **0.99** | **4%** |
| Uterus | **1.09** | 0.003 | **1.09** | 0.08 | **1.08** | 0.01 | 0.05 | 0.03 | 0.03 | **1.03** | **3%** |
| Bladder | **1.06** | 0.002 | **0.99** | 0.05 | **0.99** | 0.01 | 0.03 | 0.02 | 0.02 | **0.96** | **4%** |
| Vagina | **1.01** | 0.001 | **1.02** | 0.03 | **1.01** | 0.004 | 0.02 | 0.01 | 0.01 | 0.73 | **1%** |
| Residual soft tissues | 0.73 | 0.27 | 0.57 | 0.28 | 0.39 | 0.14 | 0.25 | 0.18 | 0.22 | 0.45 | – |
| Bone surface | 1.39 | 0.71 | 0.92 | 0.49 | 0.60 | 0.23 | 0.40 | 0.26 | 0.38 | 0.75 | – |
| Red bone marrow | 0.85 | 0.46 | 0.57 | 0.34 | 0.33 | 0.17 | 0.29 | 0.18 | 0.28 | 0.45 | – |
| Skin | 0.66 | 0.32 | 0.47 | 0.27 | 0.27 | 0.14 | 0.24 | 0.17 | 0.23 | 0.35 | – |
| COV[b] | **16%** | **12%** | **14%** | **10%** | **4%** | **19%** | **10%** | **13%** | **10%** | **16%** | – |

[a]Coefficient of variation (standard deviation × 100%/mean) across examination categories that covered the entire organ volume.
[b]Coefficient of variation (standard deviation × 100%/mean) across organs entirely inside the scan coverage.

TABLE XVI. $CTDI_{vol}$-to-organ dose conversion coefficients (*h* factors, unitless) for the **obese-class-I female phantom**. The simulations were performed for the LightSpeed VCT scanner using a tube voltage of 120 kVp, a pitch of 1.375, a beam collimation of 40 mm, and large body scan field-of-view. $CTDI_{vol}$ = 6.01 mGy/100 mAs. The *h* factors are in boldface for organs entirely inside the scan coverage.

| | Chest-abdomen-pelvis | Chest | Abdomen-pelvis | Abdomen | Pelvis | Adrenals | Liver | Kidneys | Liver to kidneys | Kidneys to bladder | COV[a] |
|---|---|---|---|---|---|---|---|---|---|---|---|
| Eyes | 0.02 | 0.02 | 0.002 | 0.002 | 0.0001 | 0.001 | 0.002 | 0.0008 | 0.002 | 0.001 | – |
| Brain | 0.02 | 0.02 | 0.002 | 0.002 | 0.0001 | 0.001 | 0.002 | 0.0009 | 0.002 | 0.001 | – |
| Pharynx-larynx | 0.67 | 0.67 | 0.02 | 0.02 | 0.001 | 0.01 | 0.02 | 0.01 | 0.02 | 0.01 | – |
| Thyroid | **1.25** | **1.24** | 0.05 | 0.05 | 0.001 | 0.02 | 0.05 | 0.02 | 0.05 | 0.02 | **0.4%** |
| Trachea-bronchi | **1.10** | **1.08** | 0.23 | 0.23 | 0.004 | 0.07 | 0.23 | 0.08 | 0.23 | 0.08 | **1%** |
| Breasts | **0.77** | **0.75** | 0.42 | 0.42 | 0.004 | 0.16 | 0.42 | 0.17 | 0.42 | 0.17 | **1.6%** |
| Thymus | **1.26** | **1.25** | 0.20 | 0.20 | 0.003 | 0.06 | 0.20 | 0.06 | 0.20 | 0.07 | **0.5%** |
| Esophagus | **0.90** | **0.88** | 0.26 | 0.26 | 0.01 | 0.10 | 0.26 | 0.11 | 0.26 | 0.11 | **2%** |
| Lungs | **1.05** | **1.02** | 0.48 | 0.48 | 0.01 | 0.17 | 0.48 | 0.18 | 0.48 | 0.18 | **2%** |
| Heart | **1.09** | **1.05** | 0.76 | 0.76 | 0.01 | 0.29 | 0.75 | 0.30 | 0.76 | 0.30 | **3%** |
| Liver | **0.85** | 0.66 | **0.77** | **0.76** | 0.04 | 0.57 | **0.75** | 0.62 | **0.76** | 0.64 | **5%** |
| Gall bladder | **1.06** | 0.81 | **0.92** | **0.91** | 0.05 | **0.77** | **0.89** | **0.83** | **0.90** | **0.85** | **9%** |
| Spleen | **0.84** | **0.71** | **0.75** | **0.75** | 0.03 | 0.59 | **0.74** | 0.62 | **0.74** | 0.63 | **6%** |
| Stomach | **0.96** | 0.76 | **0.90** | **0.89** | 0.04 | 0.73 | **0.88** | 0.77 | **0.88** | 0.78 | **3%** |
| Pancreas | **0.81** | 0.46 | **0.78** | **0.77** | 0.08 | **0.60** | **0.73** | **0.69** | **0.75** | **0.72** | **9%** |
| Adrenal glands | **0.74** | 0.46 | **0.69** | **0.68** | 0.06 | **0.55** | **0.65** | **0.61** | **0.67** | **0.63** | **9%** |
| Kidneys | **0.82** | 0.25 | **0.80** | **0.78** | 0.12 | 0.55 | **0.72** | **0.73** | **0.76** | **0.77** | **4%** |
| Large intestine | **0.86** | 0.13 | **0.84** | 0.60 | 0.47 | 0.30 | 0.45 | 0.47 | 0.49 | **0.82** | **3%** |

TABLE XVI. (*Continued*)

| | Chest-abdomen-pelvis | Chest | Abdomen-pelvis | Abdomen | Pelvis | Adrenals | Liver | Kidneys | Liver to kidneys | Kidneys to bladder | COV[a] |
|---|---|---|---|---|---|---|---|---|---|---|---|
| Small intestine | **0.89** | 0.12 | **0.88** | 0.70 | 0.54 | 0.27 | 0.49 | 0.52 | 0.53 | **0.86** | **2%** |
| Ovaries | **0.71** | 0.003 | **0.75** | 0.07 | **0.76** | 0.01 | 0.02 | 0.03 | 0.03 | **0.73** | **3%** |
| Uterus | **0.79** | 0.002 | **0.81** | 0.05 | **0.79** | 0.01 | 0.01 | 0.02 | 0.02 | **0.77** | **2%** |
| Bladder | **0.79** | 0.001 | **0.73** | 0.03 | **0.73** | 0.004 | 0.01 | 0.02 | 0.02 | **0.68** | **6%** |
| Vagina | **0.76** | 0.001 | **0.72** | 0.02 | **0.71** | 0.002 | 0.01 | 0.01 | 0.01 | **0.61** | **9%** |
| Residual soft tissues | 0.44 | 0.14 | 0.36 | 0.18 | 0.25 | 0.08 | 0.13 | 0.13 | 0.15 | 0.30 | – |
| Bone surface | 0.89 | 0.45 | 0.61 | 0.34 | 0.36 | 0.15 | 0.27 | 0.22 | 0.30 | 0.50 | – |
| Red bone marrow | 0.58 | 0.29 | 0.41 | 0.25 | 0.22 | 0.11 | 0.20 | 0.17 | 0.23 | 0.34 | – |
| Skin | 0.38 | 0.16 | 0.29 | 0.16 | 0.17 | 0.07 | 0.13 | 0.11 | 0.14 | 0.23 | – |
| COV[b] | **18%** | **20%** | **9%** | **10%** | **5%** | **18%** | **11%** | **13%** | **10%** | **12%** | – |

[a]Coefficient of variation (standard deviation × 100%/mean) across examination categories that covered the entire organ volume.
[b]Coefficient of variation (standard deviation × 100%/mean) across organs entirely inside the scan coverage.

TABLE XVII. $CTDI_{vol}$-to-organ dose conversion coefficients (*h* factors, unitless) for the **obese-class-III female phantom**. The simulations were performed for the LightSpeed VCT scanner using a tube voltage of 120 kVp, a pitch of 1.375, a beam collimation of 40 mm, and large body scan field-of-view. $CTDI_{vol}$ = 6.01 mGy/100 mAs. The *h* factors are in boldface for organs entirely inside the scan coverage.

| | Chest-abdomen-pelvis | Chest | Abdomen-pelvis | Abdomen | Pelvis | Adrenals | Liver | Kidneys | Liver to kidneys | Kidneys to bladder | COV[a] |
|---|---|---|---|---|---|---|---|---|---|---|---|
| Eyes | 0.01 | 0.01 | 0.001 | 0.001 | 0.00004 | 0.0004 | 0.001 | 0.0003 | 0.001 | 0.0004 | – |
| Brain | 0.01 | 0.01 | 0.001 | 0.001 | 0.00004 | 0.0003 | 0.001 | 0.0003 | 0.001 | 0.0003 | – |
| Pharynx-larynx | 0.34 | 0.34 | 0.01 | 0.01 | 0.0003 | 0.004 | 0.01 | 0.003 | 0.01 | 0.003 | – |
| Thyroid | 0.81 | 0.81 | 0.02 | 0.02 | 0.0004 | 0.01 | 0.02 | 0.01 | 0.02 | 0.01 | – |
| Trachea-bronchi | 0.80 | 0.79 | 0.17 | 0.17 | 0.003 | 0.05 | 0.17 | 0.04 | 0.17 | 0.04 | – |
| Breasts | **0.59** | **0.58** | 0.19 | 0.19 | 0.002 | 0.04 | 0.19 | 0.02 | 0.19 | 0.02 | **1.0%** |
| Thymus | **0.96** | **0.96** | 0.13 | 0.13 | 0.002 | 0.03 | 0.13 | 0.02 | 0.13 | 0.03 | **0.7%** |
| Esophagus | **0.64** | **0.62** | 0.21 | 0.21 | 0.01 | 0.08 | 0.20 | 0.06 | 0.21 | 0.06 | **2%** |
| Lungs | **0.80** | **0.78** | 0.34 | 0.34 | 0.01 | 0.10 | 0.33 | 0.07 | 0.33 | 0.08 | **2%** |
| Heart | **0.88** | **0.85** | 0.52 | 0.52 | 0.01 | 0.13 | 0.52 | 0.09 | 0.52 | 0.09 | **2%** |
| Liver | **0.64** | 0.48 | **0.57** | **0.57** | 0.03 | 0.39 | **0.56** | 0.34 | **0.56** | 0.36 | **6%** |
| Gall bladder | **0.79** | 0.24 | **0.77** | **0.76** | 0.06 | **0.52** | **0.73** | **0.56** | **0.75** | **0.58** | **16%** |
| Spleen | **0.53** | 0.41 | **0.49** | **0.49** | 0.03 | **0.39** | **0.48** | 0.37 | **0.48** | 0.38 | **9%** |
| Stomach | **0.72** | **0.58** | **0.67** | **0.66** | 0.03 | **0.50** | **0.65** | 0.45 | **0.65** | 0.46 | **11%** |
| Pancreas | **0.54** | 0.28 | **0.52** | **0.50** | 0.07 | **0.39** | **0.48** | **0.41** | **0.49** | **0.43** | **12%** |
| Adrenal glands | **0.53** | 0.34 | **0.50** | **0.49** | 0.05 | **0.39** | **0.47** | **0.40** | **0.48** | **0.42** | **12%** |
| Kidneys | **0.52** | 0.16 | **0.51** | **0.49** | 0.12 | 0.38 | **0.46** | **0.43** | **0.47** | **0.47** | **7%** |
| Large intestine | **0.65** | 0.06 | **0.64** | 0.41 | 0.39 | 0.21 | 0.30 | 0.32 | 0.36 | **0.60** | **4%** |
| Small intestine | **0.67** | 0.06 | **0.67** | 0.48 | 0.46 | 0.18 | 0.31 | 0.38 | 0.36 | **0.65** | **2%** |
| Ovaries | **0.47** | 0.002 | **0.47** | 0.04 | **0.46** | 0.01 | 0.02 | 0.02 | 0.02 | **0.44** | **3%** |
| Uterus | **0.53** | 0.002 | **0.53** | 0.04 | **0.52** | 0.01 | 0.01 | 0.02 | 0.02 | **0.49** | **3%** |
| Bladder | **0.50** | 0.001 | **0.50** | 0.02 | **0.50** | 0.004 | 0.01 | 0.01 | 0.01 | **0.46** | **4%** |
| Vagina | **0.48** | 0.001 | **0.49** | 0.01 | **0.49** | 0.002 | 0.01 | 0.01 | 0.01 | 0.39 | **1%** |
| Residual soft tissues | 0.35 | 0.12 | 0.29 | 0.15 | 0.19 | 0.07 | 0.12 | 0.10 | 0.13 | 0.23 | – |
| Bone surface | 0.68 | 0.38 | 0.43 | 0.25 | 0.26 | 0.11 | 0.21 | 0.12 | 0.21 | 0.33 | – |
| Red bone marrow | 0.41 | 0.23 | 0.27 | 0.17 | 0.15 | 0.08 | 0.14 | 0.08 | 0.14 | 0.20 | – |
| Skin | 0.31 | 0.14 | 0.23 | 0.13 | 0.14 | 0.06 | 0.11 | 0.08 | 0.12 | 0.17 | – |
| COV[b] | **23%** | **21%** | **17%** | **19%** | **5%** | **15%** | **19%** | **17%** | **20%** | **17%** | – |

[a]Coefficient of variation (standard deviation × 100%/mean) across examination categories that covered the entire organ volume.
[b]Coefficient of variation (standard deviation × 100%/mean) across organs entirely inside the scan coverage.

TABLE XVIII. Physical (geometric) diameters and water-equivalent diameters of different body regions of the six phantoms in this study[a].

| | Male | | | Female | | |
|---|---|---|---|---|---|---|
| | Normal | Obese class I | Obese class II | Normal | Obese class I | Obese class III |
| Physical (geometric) diameter (cm) | | | | | | |
| $d_{\text{chest}}$ | 26.8 | 32.3 | 34.5 | 27.8 | 30.5 | 35.1 |
| $d_{\text{abdomen}}$ | 25.2 | 32.0 | 35.4 | 27.0 | 30.0 | 35.7 |
| $d_{\text{pelvis}}$ | 26.7 | 31.4 | 33.7 | 28.5 | 31.3 | 36.6 |
| $d_{\text{abdomen-pelvis}}$ | 26.0 | 31.7 | 34.5 | 27.8 | 30.6 | 36.1 |
| $d_{\text{trunk}}$ | 26.3 | 31.9 | 34.4 | 27.9 | 30.6 | 35.8 |
| Water-equivalent diameter (cm) | | | | | | |
| | | | Mean energy = 62 keV[b] | | | |
| $d_{\text{w, chest}}$ | 25.3 (−6%) | 30.6 (−5%) | 32.8 (−5%) | 25.5 (−8%) | 29.2 (−4%) | 33.1 (−6%) |
| $d_{\text{w, abdomen}}$ | 25.6 (2%) | 32.4 (1%) | 35.6 (1%) | 27.1 (0%) | 30.4 (1%) | 35.9 (1%) |
| $d_{\text{w, pelvis}}$ | 28.2 (5%) | 32.6 (4%) | 35.0 (4%) | 30.0 (5%) | 32.5 (4%) | 37.8 (3%) |
| $d_{\text{w, abdomen-pelvis}}$ | 26.9 (4%) | 32.5 (3%) | 35.3 (2%) | 28.5 (3%) | 31.5 (3%) | 36.9 (2%) |
| $d_{\text{w, trunk}}$ | 26.4 (0%) | 31.9 (0%) | 34.4 (0%) | 27.6 (−1%) | 30.8 (1%) | 35.8 (0%) |
| | | | Mean energy = 83 keV[b] | | | |
| $d_{\text{w, chest}}$ | 25.1 (−7%) | 30.4 (−6%) | 32.6 (−6%) | 25.3 (−9%) | 29.0 (−5%) | 33.0 (−6%) |
| $d_{\text{w, abdomen}}$ | 25.5 (1%) | 32.3 (1%) | 35.5 (0%) | 27.0 (0%) | 30.3 (1%) | 35.9 (0%) |
| $d_{\text{w, pelvis}}$ | 27.9 (4%) | 32.4 (3%) | 34.8 (3%) | 29.7 (4%) | 32.3 (3%) | 37.6 (3%) |
| $d_{\text{w, abdomen-pelvis}}$ | 26.7 (3%) | 32.3 (2%) | 35.2 (2%) | 28.3 (2%) | 31.3 (2%) | 36.8 (2%) |
| $d_{\text{w, trunk}}$ | 26.2 (0%) | 31.7 (−1%) | 34.2 (−1%) | 27.4 (−2%) | 30.7 (0%) | 35.6 (−1%) |

[a]Percent values in parenthesis equal $\frac{d_{\text{w,region}} - d_{\text{region}}}{d_{\text{region}}} \times 100\%$.

[b]Sixty-two kilo-electron-volt is the mean energy of the 120 kVp beam at the isocenter of the GE LightSpeed VCT scanner. It was calculated after attenuating the prebowtie spectrum (at the exit of the x-ray tube and before filtration by the bowtie filter) of the 120 kVp beam by the least attenuating section of the bowtie filter (at beam angle of $0^{\circ}$). Eighty-three kilo-electron-volt is the mean energy of the prebowtie spectrum after being attenuated by 40 cm of water (representing an obese patient) and the most attenuating section of the bowtie filter (at beam angle of $\sim 27.5^{\circ}$).

TABLE XIX. Percent contributions to effective dose (hence $k$ factor) from four organ categories: inside (fully inside of the scan coverage[a]), peripheral (on the periphery of the scan coverage), distributed (extended beyond the scan coverage on both ends), and outside (fully outside of the scan coverage).

| | Male | | | Female | | |
|---|---|---|---|---|---|---|
| | Normal (%) | Obese class I (%) | Obese class II (%) | Normal (%) | Obese class I (%) | Obese class III (%) |
| **Chest-abdomen-pelvis** | | | | | | |
| Inside | 85 | 86 | 85 | 83 | 87 | 82 |
| Peripheral | 5 | 4 | 5 | 6 | 2 | 7 |
| Distributed | 10 | 10 | 10 | 11 | 11 | 11 |
| Outside | 0.02 | 0.02 | 0.02 | 0.02 | 0.03 | 0.02 |
| **Chest** | | | | | | |
| Inside | 54 | 58 | 53 | 58 | 60 | 70 |
| Peripheral | 38 | 34 | 38 | 32 | 32 | 21 |
| Distributed | 8 | 8 | 9 | 9 | 8 | 9 |
| Outside | 0.05 | 0.04 | 0.2 | 0.5 | 0.1 | 0.1 |
| **Abdomen-pelvis** | | | | | | |
| Inside | 75 | 71 | 69 | 70 | 66 | 69 |
| Peripheral | 12 | 18 | 22 | 19 | 22 | 19 |
| Distributed | 11 | 10 | 8 | 11 | 11 | 11 |
| Outside | 2 | 1 | 0.4 | 0.2 | 0.8 | 0.6 |
| **Abdomen** | | | | | | |
| Inside | 47 | 43 | 39 | 46 | 41 | 44 |
| Peripheral | 39 | 47 | 54 | 43 | 48 | 45 |
| Distributed | 9 | 9 | 7 | 9 | 9 | 9 |
| Outside | 4 | 1 | 1 | 2 | 3 | 2 |

TABLE XIX. (*Continued*)

| | Male | | | Female | | |
|---|---|---|---|---|---|---|
| | Normal (%) | Obese class I (%) | Obese class II (%) | Normal (%) | Obese class I (%) | Obese class III (%) |
| **Pelvis** | | | | | | |
| Inside | 50 | 48 | 52 | 39 | 47 | 42 |
| Peripheral | 30 | 32 | 32 | 43 | 30 | 36 |
| Distributed | 16 | 15 | 11 | 16 | 18 | 17 |
| Outside | 4 | 5 | 5 | 2 | 5 | 5 |
| **Adrenals** | | | | | | |
| Inside | 50 | 47 | 46 | 5 | 7 | 48 |
| Peripheral | 31 | 34 | 44 | 86 | 85 | 32 |
| Distributed | 17 | 17 | 6 | 7 | 7 | 18 |
| Outside | 2 | 2 | 4 | 1 | 1 | 2 |
| **Liver** | | | | | | |
| Inside | 52 | 46 | 40 | 48 | 44 | 47 |
| Peripheral | 37 | 46 | 53 | 43 | 47 | 43 |
| Distributed | 8 | 8 | 6 | 8 | 8 | 8 |
| Outside | 4 | 1 | 0.8 | 1 | 2 | 2 |
| **Kidneys** | | | | | | |
| Inside | 10 | 45 | 10 | 51 | 9 | 10 |
| Peripheral | 81 | 45 | 80 | 39 | 80 | 79 |
| Distributed | 7 | 8 | 7 | 7 | 9 | 9 |
| Outside | 2 | 2 | 3 | 3 | 2 | 2 |
| **Liver-to-kidney** | | | | | | |
| Inside | 52 | 45 | 39 | 50 | 43 | 46 |
| Peripheral | 36 | 46 | 54 | 41 | 47 | 44 |
| Distributed | 8 | 8 | 6 | 8 | 9 | 8 |
| Outside | 4 | 1 | 0.9 | 1 | 2 | 2 |
| **Kidney-to-bladder** | | | | | | |
| Inside | 45 | 40 | 43 | 75 | 50 | 56 |
| Peripheral | 37 | 46 | 46 | 13 | 38 | 32 |
| Distributed | 12 | 12 | 9 | 11 | 12 | 12 |
| Outside | 6 | 1 | 1 | 1 | 0.4 | 0.5 |

[a]Scan coverage = image coverage + over-ranging distance.

TABLE XX. Percent contributions to risk index (hence $q$ factor)[a] from four organ categories: inside (fully inside of the scan coverage[b]), peripheral (on the periphery of the scan coverage), distributed (extended beyond the scan coverage on both ends), and outside (fully outside of the scan coverage).

| | Male | | | Female | | |
|---|---|---|---|---|---|---|
| | Normal (%) | Obese class I (%) | Obese class II (%) | Normal (%) | Obese class I (%) | Obese class III (%) |
| **Chest-abdomen-pelvis** | | | | | | |
| Inside | 87 | 87 | 87 | 85 | 92 | 84 |
| Peripheral | 4 | 3 | 4 | 9 | 2 | 10 |
| Distributed | 10 | 10 | 9 | 5 | 5 | 5 |
| Outside | 0.02 | 0.02 | 0.03 | 0.02 | 0.02 | 0.02 |
| **Chest** | | | | | | |
| Inside | 54 | 57 | 55 | 78 | 85 | 78 |
| Peripheral | 36 | 33 | 34 | 18 | 12 | 18 |
| Distributed | 10 | 10 | 10 | 3 | 3 | 4 |
| Outside | 0.1 | 0.1 | 0.4 | 0.4 | 0.07 | 0.07 |
| **Abdomen-pelvis** | | | | | | |
| Inside | 78 | 76 | 80 | 51 | 46 | 50 |
| Peripheral | 13 | 15 | 12 | 41 | 46 | 42 |
| Distributed | 9 | 9 | 7 | 7 | 7 | 7 |
| Outside | 0.4 | 0.5 | 0.4 | 0.4 | 1 | 1 |

TABLE XX. (*Continued*)

| | Male | | | Female | | |
|---|---|---|---|---|---|---|
| | Normal (%) | Obese class I (%) | Obese class II (%) | Normal (%) | Obese class I (%) | Obese class III (%) |
| **Abdomen** | | | | | | |
| Inside | 31 | 29 | 29 | 24 | 19 | 22 |
| Peripheral | 58 | 60 | 61 | 68 | 73 | 70 |
| Distributed | 9 | 9 | 8 | 6 | 5 | 6 |
| Outside | 2 | 2 | 2 | 2 | 3 | 3 |
| **Pelvis** | | | | | | |
| Inside | 59 | 57 | 59 | 49 | 56 | 51 |
| Peripheral | 29 | 31 | 32 | 35 | 26 | 31 |
| Distributed | 10 | 9 | 7 | 13 | 13 | 13 |
| Outside | 2 | 2 | 2 | 3 | 5 | 5 |
| **Adrenals** | | | | | | |
| Inside | 31 | 27 | 29 | 8 | 11 | 32 |
| Peripheral | 51 | 55 | 63 | 85 | 83 | 55 |
| Distributed | 17 | 17 | 7 | 5 | 5 | 10 |
| Outside | 0.7 | 1 | 2 | 1 | 1 | 3 |
| **Liver** | | | | | | |
| Inside | 35 | 33 | 32 | 25 | 20 | 23 |
| Peripheral | 56 | 58 | 59 | 69 | 74 | 70 |
| Distributed | 8 | 8 | 7 | 5 | 4 | 5 |
| Outside | 1 | 1 | 2 | 2 | 2 | 2 |
| **Kidneys** | | | | | | |
| Inside | 15 | 27 | 13 | 40 | 14 | 18 |
| Peripheral | 77 | 63 | 78 | 46 | 78 | 72 |
| Distributed | 7 | 8 | 7 | 6 | 6 | 8 |
| Outside | 0.9 | 2 | 2 | 8 | 2 | 3 |
| **Liver-to-kidney** | | | | | | |
| Inside | 36 | 31 | 30 | 25 | 20 | 22 |
| Peripheral | 55 | 59 | 61 | 69 | 73 | 70 |
| Distributed | 8 | 8 | 7 | 5 | 5 | 5 |
| Outside | 1 | 2 | 2 | 1 | 2 | 2 |
| **Kidney-to-bladder** | | | | | | |
| Inside | 67 | 37 | 62 | 72 | 53 | 64 |
| Peripheral | 19 | 52 | 30 | 16 | 38 | 25 |
| Distributed | 10 | 10 | 7 | 9 | 8 | 10 |
| Outside | 5 | 1 | 0.3 | 4 | 0.7 | 0.9 |

[a]All phantoms were assumed to be 20 years of age for this analysis.
[b]Scan coverage = image coverage + over-ranging distance.

[1]F. V. Coakley, R. Gould, B. M. Yeh, and R. L. Arenson, "CT radiation dose: What can you do right now in your practice?" AJR, Am. J. Roentgenol. **196**, 619–625 (2011).
[2]L. Berlin, "To order or not to order a CT examination because of radiation exposure: That is the question," AJR, Am. J. Roentgenol. **196**, W216 (2011).
[3]H. Hricak, D. J. Brenner, S. J. Adelstein, D. P. Frush, E. J. Hall, R. W. Howell, C. H. McCollough, F. A. Mettler, M. S. Pearce, O. H. Suleiman, J. H. Thrall, and L. K. Wagner, "Managing radiation use in medical imaging: A multifaceted challenge," Radiology **258**, 889–905 (2011).
[4]NCRP, "Ionizing radiation exposure of the population of the United States," NCRP Report No. 160 (National Council on Radiation Protection and Measurements, Bethesda, MD, 2009).
[5]K. J. Strauss, M. J. Goske, D. P. Frush, P. F. Butler, and G. Morrison, "Image Gently Vendor Summit: Working together for better estimates of pediatric radiation dose from CT," AJR, Am. J. Roentgenol. **192**, 1169–1175 (2009).
[6]X. Li, E. Samei, W. P. Segars, G. M. Sturgeon, J. G. Colsher, G. Toncheva, T. T. Yoshizumi, and D. P. Frush, "Patient-specific radiation dose and cancer risk estimation in CT: Part II. Application to patients," Med. Phys. **38**, 408–419 (2011).
[7]X. Li, E. Samei, W. P. Segars, G. M. Sturgeon, J. G. Colsher, and D. P. Frush, "Patient-specific radiation dose and cancer risk for pediatric chest CT," Radiology **259**, 862–874 (2011).
[8]P. Shrimpton, Assessment of Patient Dose in CT, NRPB-PE/1/2004, NRPB, Chilton, 2004.
[9]W. Huda, K. M. Ogden, and M. R. Khorasani, "Converting dose-length product to effective dose at CT," Radiology **248**, 995–1003 (2008).
[10]A. C. Turner, D. Zhang, M. Khatonabadi, M. Zankl, J. J. DeMarco, C. H. Cagnon, D. D. Cody, D. M. Stevens, C. H. McCollough, and M. F. McNitt-Gray, "The feasibility of patient size-corrected, scanner-independent organ dose estimates for abdominal CT exams," Med. Phys. **38**, 820–829 (2011).
[11]AAPM, "The measurement, reporting, and management of radiation dose in CT," AAPM Report No. 96 (American Association of Physicists in Medicine, College Park, MD, 2008).
[12]J. A. Christner, J. M. Kofler, and C. H. McCollough, "Estimating effective dose for CT using dose-length product compared with using organ doses:

Consequences of adopting International Commission on Radiological Protection publication 103 or dual-energy scanning," AJR, Am. J. Roentgenol. **194**, 881–889 (2010).
[13]A. C. Turner, M. Zankl, J. J. DeMarco, C. H. Cagnon, D. Zhang, E. Angel, D. D. Cody, D. M. Stevens, C. H. McCollough, and M. F. McNitt-Gray, "The feasibility of a scanner-independent technique to estimate organ dose from MDCT scans: Using CTDIvol to account for differences between scanners," Med. Phys. **37**, 1816–1825 (2010).
[14]AAPM, "Size-specific dose estimates (SSDE) in pediatric and adult body CT examinations," AAPM Report No. 204 (American Association of Physicists in Medicine, College Park, MD, 2011).
[15]http://www.cdc.gov/obesity/data/trends.HTML.
[16]W. E. Lorensen and H. E. Cline, "Marching cubes: A high resolution 3D surface construction algorithm," *Proceedings of the 14th Annual Conference on Computer Graphics and Interactive Techniques* (Association for Computing Machinery, New York, NY, 1987), pp. 163–169.
[17]W. P. Segars, G. Sturgeon, S. Mendonca, J. Grimes, and B. M. Tsui, "4D XCAT phantom for multimodality imaging research," Med. Phys. **37**, 4902–4915 (2010).
[18]M. F. Beg, M. I. Miller, A. Trouve, and L. Younes, "Computing large deformation metric mappings via geodesic flows of diffeomorphisms," Int. J. Comput. Vis. **61**, 139–157 (2005).
[19]W. P. Segars, G. Sturgeon, X. Li, L. Cheng, C. Ceritoglu, J. T. Ratnanather, M. I. Miller, B. M. W. Tsui, D. P. Frush, and E. Samei, "Patient specific computerized phantoms to estimate dose in pediatric CT," *Proc. SPIE* **7258**, 72580H (2009).
[20]D. J. Tward, C. Ceritoglu, A. Kolasny, G. M. Sturgeon, W. P. Segars, M. I. Miller, and J. T. Ratnanather, "Patient specific dosimetry phantoms using multichannel LDDMM of the whole body," Int. J. Biomed. Imaging **2011**, 481064 (2011).
[21]D. J. Tward, C. Ceritoglu, G. Sturgeon, W. P. Segars, M. I. Miller, and J. T. Ratnanather, "Generating patient-specific dosimetry phantoms with whole-body diffeomorphic image registration," *Proceedings of the 37th Annual NorthEast Bioengineering Conference* (Institute of Electrical and Electronics Engineers, Troy, NY, 2011).
[22]ICRP, "Basic anatomical and physiological data for use in radiological protection: Reference values," ICRP Publication 89 (International Commission on Radiological Protection, New York, 2002).
[23]ICRP, "The 2007 Recommendations of the International Commission on Radiological Protection," ICRP Publication 103 (International Commission on Radiological Protection, Essen, Germany, 2007).
[24]X. Li, E. Samei, W. P. Segars, G. M. Sturgeon, J. G. Colsher, G. Toncheva, T. T. Yoshizumi, and D. P. Frush, "Patient-specific radiation dose and cancer risk estimation in CT: Part I. Development and validation of a Monte Carlo program," Med. Phys. **38**, 397–407 (2011).
[25]A. J. van der Molen and J. Geleijns, "Overranging in multisection CT: Quantification and relative contribution to dose–comparison of four 16-section CT scanners," Radiology **242**, 208–216 (2007).
[26]M. Cristy and K. F. Eckerman, "Specific absorbed fractions of energy at various ages from internal photon sources," ORNL/TM-8381/Vol. I–VII (Oak Ridge National Laboratory, Oak Ridge, TN, 1987).
[27]C. Lee, A. P. Shah, and W. E. Bolch, "An assessment of bone marrow and bone endosteum dosimetry methods for photon sources," Phys. Med. Biol. **51**, 5391–5407 (2006).
[28]D. J. Brenner, "Effective dose: A flawed concept that could and should be replaced," Br. J. Radiol. **81**, 521–523 (2008).
[29]National Research Council, *Health Risks from Exposure to Low Levels of Ionizing Radiation—BEIR VII* (The National Academies Press, Washington, DC, 2006).
[30]B. Rosner, *Fundamentals of Biostatistics*, 6th ed. (Thomson-Brooks/Cole, Belmont, CA, 2006).
[31]T. S. Cook, S. Zimmerman, A. D. Maidment, W. Kim, and W. W. Boonn, "Automated extraction of radiation dose information for CT examinations," J. Am. Coll. Radiol. **7**, 871–877 (2010).
[32]X. Li, D. Zhang, and B. Liu, "Automated extraction of radiation dose information from CT dose report images," AJR, Am. J. Roentgenol. **196**, W781–W783 (2011).
[33]O. Christianson, X. Li, D. F. Frush, and E. Samei, "Automated size-specific CT dose monitoring system: Assessing variability in CT dose," Med. Phys. (in press).
[34]E. S. Amis, Jr., P. F. Butler, K. E. Applegate, S. B. Birnbaum, L. F. Brateman, J. M. Hevezi, F. A. Mettler, R. L. Morin, M. J. Pentecost, G. G. Smith, K. J. Strauss, and R. K. Zeman, "American College of Radiology white paper on radiation dose in medicine," J. Am. Coll. Radiol. **4**, 272–284 (2007).
[35]D. Brenner and W. Huda, "Effective dose: A useful concept in diagnostic radiology?" Radiat. Prot. Dosim. **128**, 503–508 (2008).
[36]C. J. Martin, "Effective dose: How should it be applied to medical exposures?" Br. J. Radiol. **80**, 639–647 (2007).
[37]C. J. Martin, "The application of effective dose to medical exposures," Radiat. Prot. Dosim. **128**, 1–4 (2008).
[38]C. Borras, W. Huda, and C. G. Orton, "Point/counterpoint: The use of effective dose for medical procedures is inappropriate," Med. Phys. **37**, 3497–3500 (2010).
[39]W. Huda, J. V. Atherton, D. E. Ware, and W. A. Cumming, "An approach for the estimation of effective radiation dose at CT in pediatric patients," Radiology **203**, 417–422 (1997).
[40]J. J. DeMarco, C. H. Cagnon, D. D. Cody, D. M. Stevens, C. H. McCollough, M. Zankl, E. Angel, and M. F. McNitt-Gray, "Estimating radiation doses from multidetector CT using Monte Carlo simulations: Effects of different size voxelized patient models on magnitudes of organ and effective dose," Phys. Med. Biol. **52**, 2583–2597 (2007).
[41]A. Ding, M. M. Mille, T. Liu, P. F. Caracappa, and X. G. Xu, "Extension of RPI-adult male and female computational phantoms to obese patients and a Monte Carlo study of the effect on CT imaging dose," Phys. Med. Biol. **57**, 2441–2459 (2012).
[42]J. Menke, "Comparison of different body size parameters for individual dose adaptation in body CT of adults," Radiology **236**, 565–571 (2005).
[43]W. Huda, E. M. Scalzetti, and M. Roskopf, "Effective doses to patients undergoing thoracic computed tomography examinations," Med. Phys. **27**, 838–844 (2000).
[44]W. Huda, A. Sterzik, S. Tipnis, and U. J. Schoepf, "Organ doses to adult patients for chest CT," Med. Phys. **37**, 842–847 (2010).
[45]J. Hsieh, *Computed Tomography: Principles, Design, Artifacts, and Recent Advances* (SPIE Optical Engineering Press, Bellingham, WA, 2003).
[46]X. Li, E. Samei, R. Raupach, B. Schmidt, X. Zhou, C. H. Williams, W. P. Segars, E. K. Paulson, and D. P. Frush, "The effect of tube current modulation on dose and risk conversion coefficients in CT," *97th Scientific Assembly and Annual Meeting of the Radiological Society of North America* (Radiological Society of North America, Chicago, IL, 2011).
[47]BMI Classification, World Health Organization. http://apps.who.int/bmi/index.jsp?introPage=intro_3.html. Last accessed December 2011.